

Cleavage factor 25 deregulation contributes to pulmonary fibrosis through alternative polyadenylation

Tingting Weng,¹ Junsuk Ko,¹ Chioniso P. Masamha,¹ Zheng Xia,² Yu Xiang,¹ Ning-yuan Chen,¹ Jose G. Molina,¹ Scott Collum,¹ Tinne C. Mertens,¹ Fayong Luo,¹ Kemly Philip,¹ Jonathan Davies,³ Jingjing Huang,⁴ Cory Wilson,¹ Rajarajan A. Thandavarayan,⁵ Brian A. Bruckner,⁵ Soma S.K. Jyothula,⁶ Kelly A. Volcik,¹ Lei Li,² Leng Han,¹ Wei Li,² Shervin Assassi,⁶ Harry Karmouty-Quintana,¹ Eric J. Wagner,⁷ and Michael R. Blackburn¹

¹Department of Biochemistry and Molecular Biology, McGovern Medical School at UTHealth, Houston, Texas, USA. ²Dan L Duncan Comprehensive Cancer Center, Baylor College of Medicine Houston, Texas, USA. ³Division of Neonatal-Perinatal Medicine, Department of Pediatrics, Baylor College of Medicine, Houston, Texas, USA. ⁴The Second Affiliated Hospital of Nanjing Medical University, Nanjing, Jiangsu, China. ⁵Houston Methodist DeBakey Transplant Center, Houston Methodist Hospital, Houston, Texas, USA. ⁶Department of Internal Medicine, McGovern Medical School at UTHealth, Houston, Texas, USA. ⁷Department of Biochemistry and Molecular Biology, University of Texas Medical Branch at Galveston, Galveston, Texas, USA.

Idiopathic pulmonary fibrosis (IPF) is a deadly disease with a poor prognosis and few treatment options. Pathological remodeling of the extracellular matrix (ECM) is a key factor that drives the disease pathogenesis, although the underlying mechanisms remain unknown. Alternative polyadenylation (APA) has recently been shown to play a major role in cellular responses to stress by driving the expression of fibrotic factors through the alteration of miRNA sensitivity, but a connection to IPF has not been established. Here, we demonstrated that CFIm25, a global regulator of APA, was downregulated in the lungs of patients with IPF and mice with pulmonary fibrosis, with its expression selectively reduced in α -smooth muscle actin-positive (α -SMA-positive) fibroblasts. Following CFIm25 knockdown in healthy human lung fibroblasts, we identified 808 genes with shortened 3'-UTRs, including those involved in the TGF- β signaling pathway, the Wnt signaling pathway, and cancer pathways. The expression of key profibrotic factors was suppressed by CFIm25 overexpression in IPF fibroblasts. Finally, we demonstrated that deletion of CFIm25 in fibroblasts or myofibroblast precursors using either the *Col1a1* or the *Foxd1* promoter enhanced pulmonary fibrosis after bleomycin exposure. Collectively, our results identified CFIm25 downregulation as an important mechanism for elevating profibrotic gene expression in pulmonary fibrosis.

Introduction

Idiopathic pulmonary fibrosis (IPF) is a deadly disease that is initiated by repetitive epithelial and endothelial cell injury and progresses with rapid proliferation and differentiation of myofibroblasts. Myofibroblasts are the major source of extracellular matrix (ECM) proteins, including collagen and fibronectin (FN) (1, 2). Excessive accumulation of these ECMs around damaged and inflamed tissue leads to the thickening and stiffening of lung tissue and dampens the air-liquid interface (1, 2). The development of pulmonary fibrosis is accompanied by sophisticated changes in gene expression, including those involved in the TGF- β and Wnt signaling pathways, coagulation, angiogenesis, oxidative stress, and development (3, 4). Overexpression of key growth factors and proinflammatory cytokines including TGF- β , ILs (e.g., IL-1 β , IL-6, and IL-17), and TNF promote the proliferation and differentiation of myofibroblasts and ECM deposition (1, 5). Despite these observations, the mechanisms that trigger the overexpression of these key factors and profibrotic proteins are not fully understood, especially at the level of RNA regulation.

Polyadenylation has recently gained attention as an important RNA regulation process required for mRNA stability, translation, and translocation. The majority of human genes contain more than 1 poly(A) site, and polyadenylation gives rise to transcripts with varied 3'-UTR lengths and in some cases an altered reading frame, a process known as alternative polyadenylation (APA) (6, 7). The distal canonical poly(A) site is more frequently used in healthy cells, leading to transcripts with long 3'-UTRs that contain numerous regulatory elements. However, recent studies have shown that in highly proliferating or differentiating cells, there is a global distal-to-proximal shift in APA site selection, generating truncated transcripts with shorter 3'-UTRs (7, 8). These shorter variants escape miRNA recognition and AU-rich element-related (ARE-related) repression and are normally more stable and have increased protein translation (8, 9). The selection of poly(A) sites (PASs) can be determined not only by adjacent sequence elements but also by the level of polyadenylation protein complexes. Several protein complexes are needed for poly(A) signal recognition, cleavage, and addition of a poly(A) tail, including cleavage and polyadenylation specificity factor (CPSF), cleavage stimulation factor (CSTF), cleavage factor Im (CFIm), and cleavage factor II_m (CFII_m). Downregulation of CFIm25, a key component of CFIm that recognizes UGUA motifs upstream of the cleavage site, induces global shortening of mRNAs (8, 9) and is recognized as a novel mechanism that increases the expression of sev-

Conflict of interest: The authors have declared that no conflict of interest exists.

Copyright: © 2019, American Society for Clinical Investigation.

Submitted: May 9, 2018; **Accepted:** February 26, 2019; **Published:** April 8, 2019.

Reference information: *J Clin Invest.* 2019;129(5):1984–1999.

<https://doi.org/10.1172/JCI122106>.

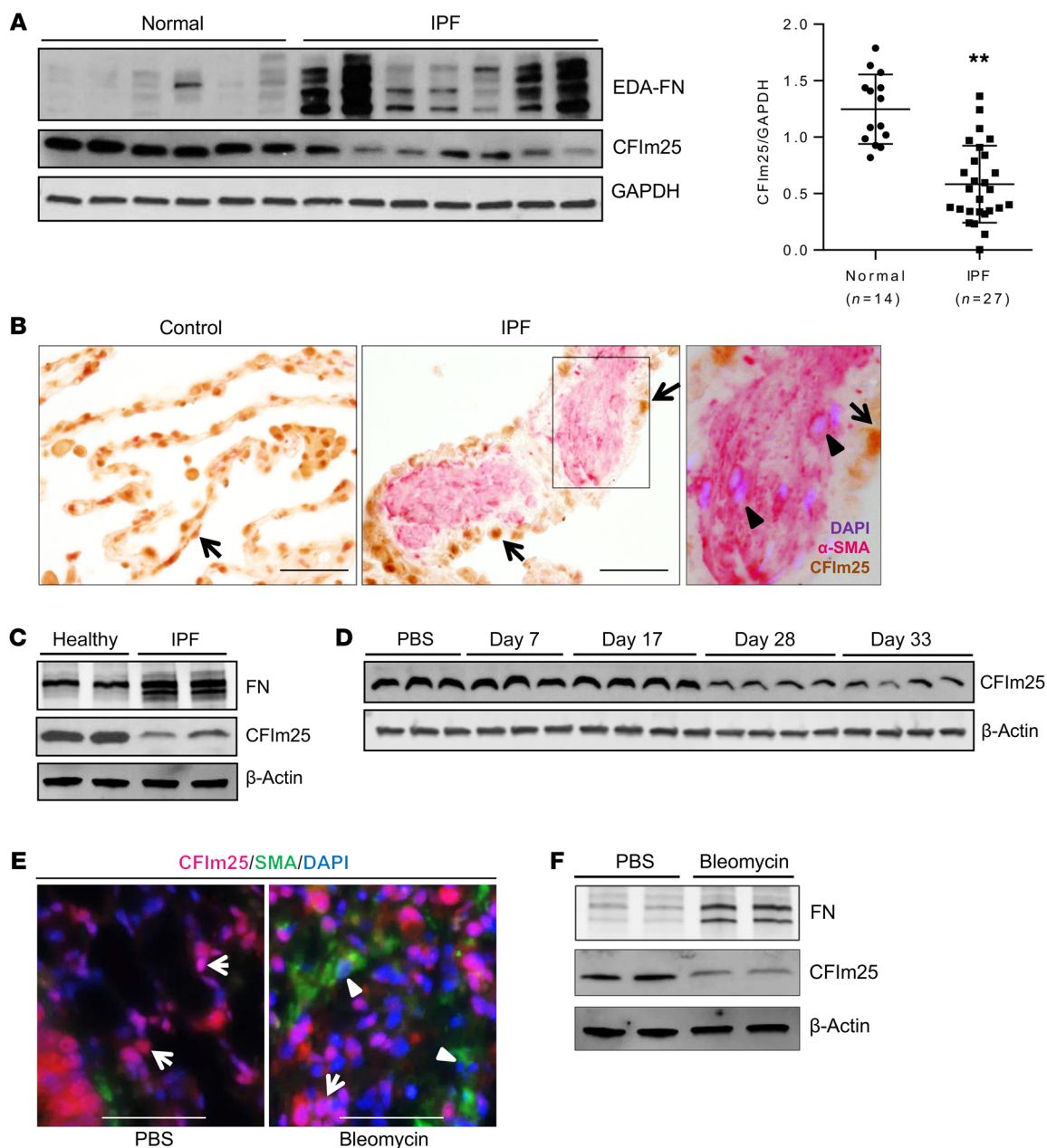


Figure 1. CFIm25 is downregulated in fibrotic lungs. (A) A representative Western blot showing protein expression of CFIm25, FN, and GAPDH from 6 healthy and 7 IPF lung specimens. CFIm25 densitometric analysis shows significantly downregulated CFIm25 levels in IPF lungs. $**P < 0.01$, by unpaired *t* test versus healthy control. (B) Immunohistochemistry for CFIm25 (brown) and α -SMA (pink) showing cellular localization in control and IPF lung specimens. Arrow indicates CFIm25-positive cells. Arrowhead indicates α -SMA-positive but CFIm25-negative cells. Scale bars: 100 μ m. Original magnification $\times 100$. (C) Western blot shows CFIm25, FN, and β -actin protein expression levels in primary fibroblast lines derived from healthy or IPF lungs. (D–F) Mice were i.p. injected with PBS or bleomycin biweekly for 4 weeks. (D) Western blotting was performed to analyze the protein expression of CFIm25 in whole-lung lysates on day 33 after PBS, or 7, 17, 28, and 33 days after the first bleomycin exposure. The different lanes represent samples collected from distinct mice. β -Actin was used as a protein loading control. (E) Immunofluorescence was carried out to determine CFIm25 (pink) and α -SMA (green) colocalization in lungs from mice exposed to PBS or bleomycin for 33 days. Arrows indicate CFIm25-positive cells; arrowheads indicate α -SMA-positive but CFIm25-negative cells. Scale bars: 100 μ m. (F) Primary fibroblasts were isolated from day-33 PBS or bleomycin-injected mouse lungs. Western blotting was performed to determine CFIm25, FN, and β -actin protein levels.

eral known oncogenes and enhances cancer cell proliferation (8). Pulmonary fibrosis is a disease with extensive cell proliferation and differentiation that shares many features similar to those of cancer. Although massive RNA shortening has been reported in several human cancers, the role of APA in fibrotic lungs and its involvement in the progression of pulmonary fibrosis are not fully understood.

In the current study, we sought to understand whether APA is involved in the regulation of profibrotic genes during the pathogenesis of pulmonary fibrosis. We first characterized the expression of CFIm25 in the lungs of humans and mice with pulmonary fibrosis and observed that this protein was downregulated in fibroblasts. Next, using RNA-Seq, we identified profibrotic

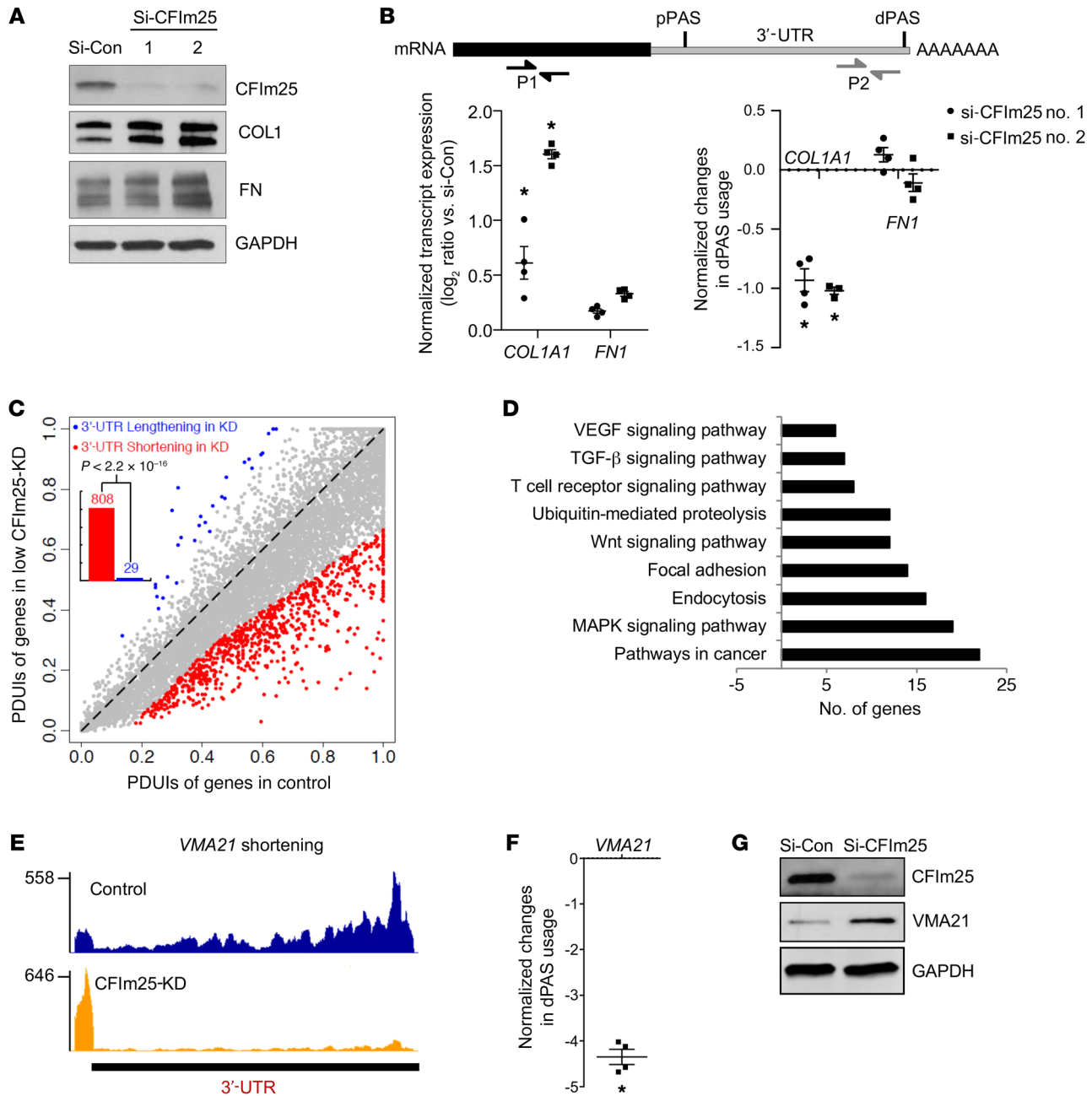


Figure 2. RNA-Seq identifies CFIm25 target genes involved in important fibrotic and cancer pathways. (A) Western blot analysis of CFIm25, COL1, and FN expression in healthy human fibroblasts (CCD8-Lu) transfected with control siRNA (si-Con) or siRNAs targeting CFIm25 (si-CFIm25). GAPDH was used as a loading control. (B) Diagram shows pPAS and dPAS, and 2 sets of primers designed to target the translated region (P1) and distal region (P2) of the 3'-UTR. qRT-PCR was performed to demonstrate *COL1A1* and *FN1* transcript expression (lower left panel) and dPAS usage (lower right panel) after knockdown of CFIm25 using 2 different siRNAs (no. 1 and no. 2). Results in the lower left panel are shown as \log_2 (fold changes vs. control siRNA-transfected samples) \pm SEM ($n = 3$ biological replicates), and results in the lower right panel are shown as the \log_2 ratio of (percentage of long transcript in si-CFIm25/percentage of long transcript in si-Con). $*P < 0.05$, by 1-sample t test versus 0. (C) Scatterplot of percentage PDUIs in control and CFIm25-knockdown cells, in which mRNAs were significantly shortened ($n = 808$) or lengthened ($n = 29$) after CFIm25 knockdown in CCD8-Lu cells. (D) Functional annotation assay of CFIm25 targets. (E) RNA-Seq read density for 3'-UTR, terminal exon, and upstream exon(s) of *VMA21* in control or CFIm25 siRNA-transfected CCD8-Lu cells. Numbers on the x axis indicate the RNA-Seq read coverage. (F) qRT-PCR was performed to demonstrate dPAS usage of *VMA21*. $n = 3$. $*P < 0.01$, by 1-sample t test versus 0. (G) Western blotting was used to verify *VMA21* expression after CFIm25 knockdown in CCD8-Lu cells. KD, knockdown.

factors and pathways targeted by CFIm25 and determined the role of CFIm25 as a regulator of fibroblast-to-myofibroblast differentiation. Moreover, using genetically modified mice, we found that downregulation of CFIm25 in myofibroblast pre-

cursors exaggerates bleomycin-induced pulmonary fibrosis in association with APA of genes in key pathways that regulate pulmonary fibrosis. Taken together, our data revealed CFIm25 deregulation and APA as mechanisms contributing to the devel-

opment of pulmonary fibrosis. Identifying this pathway in the pathogenesis of pulmonary fibrosis opens up a new line of investigation for the treatment of fibrotic diseases such as IPF.

Results

CFIm25 is downregulated in the lungs of patients with IPF and mice exposed to bleomycin. Recently, we demonstrated that the polyadenylation factor called cleavage factor I m25 (CFIm25) is a major regulator of APA (8). To understand whether a global APA event is presented in the progression of pulmonary fibrosis, we examined the expression of CFIm25 in the lungs of healthy donors and patients with IPF. We observed significant downregulation of CFIm25 in the lungs of patients with IPF (Figure 1A). We then selected IPF lung samples with different levels of FN, a marker for pulmonary fibrosis, and assessed the protein levels of all 3 CFIm components (CFIm25, CFIm59, and CFIm68) in these samples. We found that the protein levels of CFIm25 were negatively correlated with those of FN (Supplemental Figure 1A; supplemental material available online with this article; <https://doi.org/10.1172/JCI122106DS1>). Similarly, the protein expression levels of CFIm59 and CFIm68 decreased as FN levels increased (Supplemental Figure 1B), suggesting that the overall expression level of the CFIm complex is decreased in the lungs of patients with pulmonary fibrosis. Dual-immunohistochemistry was used to determine cell types exhibiting decreased CFIm25 expression. We found that CFIm25 was ubiquitously expressed in the nucleus of the majority of cells (including epithelial cells and macrophages), except smooth muscle cells in healthy lungs (Figure 1B, arrow and Supplemental Figure 1C), but was selectively downregulated in cells within fibrotic foci that expressed α -smooth muscle actin (α -SMA), a marker for myofibroblasts (Figure 1B, arrowhead, and Supplemental Figure 1C). In addition, *in vitro* studies using primary fibroblasts derived from a patient with IPF (LL97A) and from healthy lung tissue (CCD8-Lu) revealed that CFIm25 (Figure 1C), as well as CFIm59 and CFIm68 (Supplemental Figure 1B), were downregulated in IPF fibroblasts.

The configuration of the polyadenylation signals in terms of sequence and position between human and mouse orthologs is significantly conserved (10), suggesting that APA is an evolutionarily conserved cellular process. To understand whether similar biological processes are implicated in a mouse model of pulmonary fibrosis, we examined the protein expression of CFIm components in the lungs of mice exposed to bleomycin. We found that the expression of CFIm25 was decreased in whole-lung homogenates by day 28 following bleomycin exposure in our model of repeated systemic exposure to bleomycin (Figure 1D). The protein levels of CFIm59, but not CFIm68 (Supplemental Figure 2A), were also markedly downregulated in the lungs of mice exposed to bleomycin on day 33 of the protocol. Both dual-immunofluorescence (Figure 1E) and dual-immunohistochemistry (Supplemental Figure 2B) showed decreased CFIm25 immunoreactivity in α -SMA-expressing myofibroblasts. Moreover, the expression of all 3 components of CFIm was decreased in primary fibroblasts isolated from bleomycin-exposed mice (Figure 1F and Supplemental Figure 2C), further confirming the downregulation of CFIm25 in differentiated myofibroblasts. Taken together, our findings suggest that expression of the CFIm complex is downregulated in the

lungs of IPF patients and mice with pulmonary fibrosis, with the key component of the complex, CFIm25, being selectively downregulated in α -SMA-expressing myofibroblasts.

Knockdown of CFIm25 is sufficient to induce fibrotic marker expression in healthy lung fibroblasts. The depletion of any of the 3 components of CFIm, but most notably CFIm25, is known to cause 3'-UTR shortening in cancer cells (8). We thus hypothesized that the deregulation of CFIm25 in myofibroblasts could be associated with global APA changes in these cells, which could impact the expression of genes involved in the pathogenesis of pulmonary fibrosis. To begin to test this hypothesis, we examined the impact of decreased CFIm25 expression on APA in healthy lung fibroblasts using siRNA to knock down CFIm25. Doing this was sufficient to lead to increases in both collagen 1 (COL1) and FN expression (Figure 2A). Unlike glioblastoma cancer cells (8), proliferation was not enhanced but was instead suppressed in human lung fibroblasts after CFIm25 depletion (Supplemental Figure 5C), while fibroblast differentiation was not affected, and the expression of α -SMA was not changed (data not shown). Deregulation of CFIm25 typically upregulates targeted gene translation by promoting 3'-UTR shortening (8). To understand whether knockdown of CFIm25 directly causes collagen type I α 1 chain (*COL1A1*) and *FNI* 3'-UTR shortening, we used quantitative real-time PCR (qRT-PCR) to monitor the use of the distal PAS (dPAS) normalized to total mRNA levels. Two pairs of primers were designed, with one targeting the ORF of transcripts to represent the total transcript level and the other targeting sequences just before the dPAS to detect long transcripts that use the dPAS (Figure 2B, diagram). As shown in Figure 2B, *COL1A1* had significantly increased transcript levels and decreased usage of the dPAS after both siRNA treatments, suggesting that knockdown of CFIm25 directly leads to 3'-UTR shortening of *COL1A1* (Figure 2B). However, the transcript levels and dPAS usage of *FNI* were not significantly altered after CFIm25 knockdown (Figure 2B), possibly because it is regulated by another indirect mechanism. Taken together, our data demonstrate that knockdown of CFIm25 is sufficient to induce fibrotic marker expression in healthy lung fibroblasts by promoting 3'-UTR shortening through APA.

RNA-Seq identified key components of TGF- β and Wnt signaling pathways as CFIm25 targets. To globally identify targets of CFIm25, we performed high-depth ($>3.0 \times 10^8$ reads) RNA-Seq after knocking down CFIm25 in parallel with a control knockdown in primary healthy human lung fibroblasts (CCD8-Lu). The *de novo* 3'-UTR alterations between control and CFIm25-knockdown cells were identified using the bioinformatics algorithm dynamic analysis of alternative polyadenylation from RNA-Seq (DaPars) as previously described (8, 11). DaPars identified 808 transcripts that have a significant shift in 3'-UTR usage to proximal PASs (pPASs) in response to CFIm25 depletion compared with only 29 transcripts that have a significant shift in 3'-UTR usage to dPASs (Figure 2C and Supplemental Table 1). This finding is consistent with previous studies showing that the function of CFIm25 is to enhance the use of PASs distal to the stop codon and at the same time repress the use of those that are proximal (8). Moreover, a functional annotations assay suggested that the 808 CFIm25 targets were involved in important pathways including cancer, TGF- β , Wnt, and HIF-1 α signaling (Figure 2D). To verify the accuracy of the RNA-Seq data,

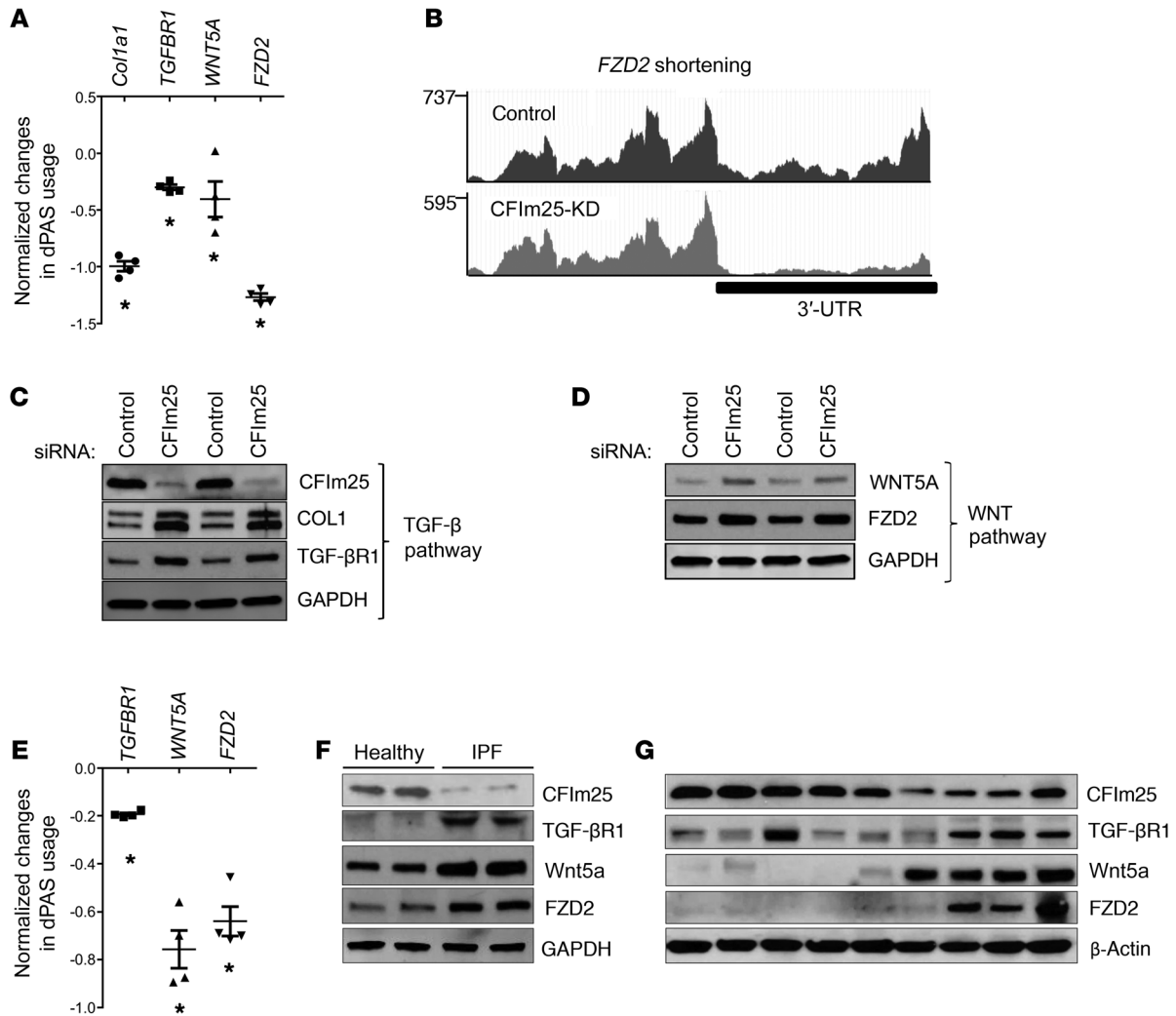


Figure 3. TGF- β and Wnt5A pathways are activated in CFIm25-knockdown fibroblasts. (A) The dPAS usage of CFIm25 targets involved in TGF- β (*TGFBFR1*) and Wnt (*WNT5A* and *FZD2*) pathways was verified by qRT-PCR. $n = 3$ biological replicates. $*P < 0.05$ one sample t test versus 0. (B) RNA-Seq read density for a representative target (*FZD2*) is shown in control and CFIm25-knockdown CCD8-Lu cells. $n = 3$ biological replicates. $P < 0.05$, by 1-sample t test versus 0. Western blotting was performed to determine protein levels of (C) CFIm25 and TGF- β R1 and (D) Wnt5A and FZD2 in CFIm25-knockdown CCD8-Lu cells. (E) The dPAS usage of CFIm25 targets was determined using qRT-PCR in primary healthy (CCD8-Lu) or IPF fibroblasts (LL97A). $n = 3$ biological replicates. $*P < 0.05$, by 1-sample t test versus 0. (F and G) Western blotting was performed to determine protein levels of CFIm25, TGF- β R1, Wnt5A, and FZD2 in primary healthy (CCD8-Lu) and IPF fibroblasts (LL97A) (F) and IPF lungs with different levels of CFIm25 (G).

the RNA-Seq read density for the 3'-UTR, terminal exon, and upstream exon(s) of vacuolar ATPase assembly factor (*VMA21*), a well-characterized CFIm25 target, were examined and shown to confirm APA (Figure 2E). In addition, qRT-PCR was performed to confirm decreased dPAS usage of *VMA21* after CFIm25 depletion (Figure 2F). Since 3'-UTR shortening normally leads to increased translation due to the loss of miRNA-binding sites and/or AREs, we performed Western blot analysis and confirmed a substantial increase in *VMA21* protein levels following CFIm25 knockdown (Figure 2G). With our model, 3'-UTR shortening of target genes may release miRNAs that were previously bound to their 3'-UTR, and the released miRNAs may in turn be directed to repress other genes (12). To test this, the number of miRNA-binding sites lost as a result of 3'-UTR shortening in CFIm25-knockdown cells was calculated, and 209 miRNAs were found to have lost binding sites

because of APA lead shortening. The top 20 miRNAs are listed in Supplemental Table 2, and 10 of these 20 miRNAs (highlighted in bold) are known to be involved in tissue fibrosis or fibroblast proliferation and differentiation, suggesting that CFIm25 depletion-led 3'-UTR shortening may play another role by releasing profibrotic miRNAs that promotes tissue fibrosis. In addition, we compared the APA genes from the CFIm25 knockdown with previously published IPF gene signatures (13) and the APA gene list in glioblastoma cancer cells (8) (Supplemental Figure 4). We identified 159 differentially expressed genes in CFIm25-knockdown fibroblasts as an IPF gene signature (Supplemental Table 3); however, not many APA genes overlapped with the IPF gene signatures, suggesting that many IPF genes may be regulated indirectly by APA (Supplemental Figure 4A). We also identified 458 common APA genes between CFIm25-knockdown cancer cells and lung

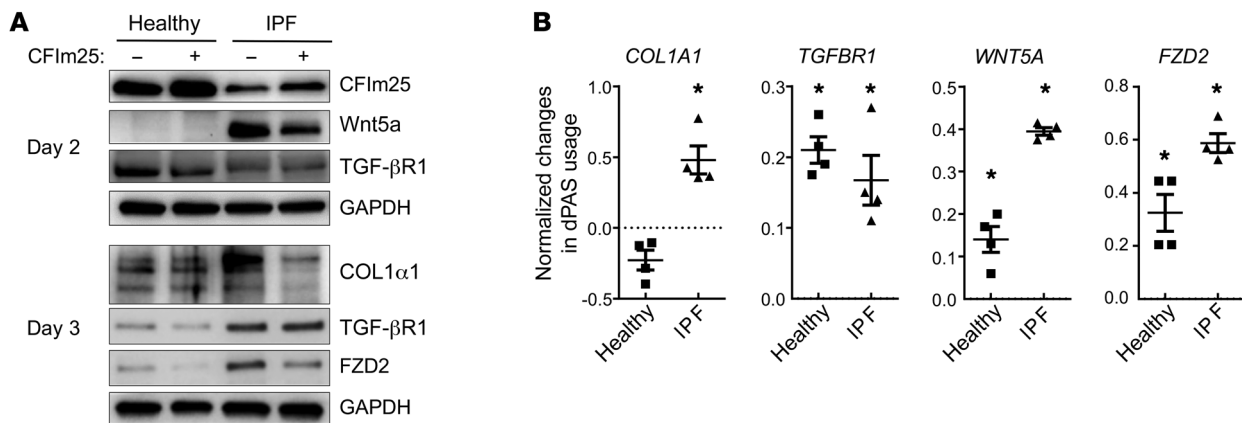


Figure 4. CFIm25 overexpression results in 3'-UTR lengthening and decreased protein expression of target genes. Primary fibroblasts isolated from healthy and IPF lungs were electroporated with empty or CFIm25-overexpressing pCDNA3.1 plasmids. Two or three days after transfection, cells were collected for (A) Western blotting to determine the protein levels of CFIm25 and its target genes and (B) qRT-PCR to determine the dPAS usage of the CFIm25 targets *COL1A1*, *TGFBR1*, *WNT5A*, and *FZD2*. $n = 3$ biological replicates. * $P < 0.05$, by 1-sample t test versus 0.

fibroblasts (Supplemental Figure 4B), and these included genes involved in cancer pathways and Wnt pathways (Figure 2D). Collectively, these results indicate a major role of CFIm25 in ensuring the use of dPAs and suggest that deregulation of CFIm25 is a mechanism that can lead to 3'-UTR shortening and the upregulation of gene expression in lung fibroblasts.

Examination of RNA-Seq findings identified numerous genes that have been shown to be involved in pulmonary fibrosis in which APA occurred in association with decreased CFIm25 levels (Supplemental Figure 3, A and B). qRT-PCR and immunoblot analyses confirmed that *COL1A1*, TGF- β receptor 1 (*TGFBR1*), Wnt family member 5A (*WNT5A*), and frizzled class receptor 2 (*FZD2*) underwent 3'-UTR shortening (Figure 3, A and B) and exhibited increased protein expression (Figure 3, C and D). These results demonstrate that a reduction in CFIm25 expression is sufficient to cause increased expression of proteins that are known to be profibrotic. To gain an understanding of whether CFIm25 is functioning in human disease, we performed qRT-PCR to determine dPAS usage in primary fibroblasts derived from a patient with IPF (LL97A) and from healthy lung tissue (CCD8-Lu) and detected significant shifting from dPAS to pPAS usage for *TGFBR1*, *WNT5A*, and *FZD2* in the primary IPF fibroblasts compared with healthy fibroblasts (Figure 3E). Consistent with their 3'-UTR shortening, we also detected an increase in protein expression of these genes in IPF fibroblasts (Figure 3F). It is important to note that the transcript levels of these genes were not increased (Supplemental Figure 5, A and B), suggesting that their enhanced protein expression was regulated posttranscriptionally. Interestingly, in correlation with lower CFIm25 levels, we also detected higher levels of TGF- β R1, Wnt5A, and FZD2 protein expression in IPF lung lysates (Figure 3G). Taken together, these findings suggest that downregulation of CFIm25 is able to activate fibrotic pathways that promote excessive expression of profibrotic factors from fibroblasts.

CFIm25 overexpression rescues IPF fibroblasts. To understand whether the fibrotic phenotype of CFIm25 knockdown can be reversed by CFIm25 overexpression, we constructed a CFIm25 overexpression (OE) plasmid by inserting the human CFIm25

gene into the pCDNA3.1 plasmid. An empty plasmid without any insertion was used as a control. We detected successful CFIm25 OE in fibroblasts transfected with the CFIm25 OE plasmid (Figure 4A) and 3'-UTR lengthening of the CFIm25 target genes *COL1A1*, *TGFBR1*, *WNT5A*, and *FZD2* (Figure 4B). Consistent with their 3'-UTR lengthening, the protein expression of Wnt5A was decreased 2 days after CFIm25 OE in IPF fibroblasts, and that of COL1 α 1 and FZD2 was decreased 3 days after CFIm25 OE in IPF fibroblasts (Figure 4A). Overall, our data indicate that the IPF fibroblast phenotype can be rescued by augmenting the expression of CFIm25.

Downregulation of CFIm25 in fibroblast precursors exaggerates bleomycin-induced pulmonary fibrosis. We next developed conditional knockout mice to examine the *in vivo* role of CFIm25 in the development of pulmonary fibrosis. We generated *Col1a1-CreER-CFIm25^{fl/fl}* mice by crossing *CFIm25^{fl/fl}* mice with *Col1a1-CreER* mice, thus allowing us to knock out CFIm25 expression in *Col1a1*-expressing cells, including fibroblasts, in an inducible manner. Although the *Col1a1-CreER* mice are reported to have high Cre activity in osteoblasts and odontoblasts, other studies have used these mice to successfully knock out genes in lung fibroblasts (14). Four- to five-week-old mice were treated with tamoxifen for five consecutive days to induce Cre expression. We observed a reduction in CFIm25 in Cre-positive cells in the fibrotic lesions (Supplemental Figure 6, arrow). To confirm the fibroblast-specific targeting of CFIm25, primary lung fibroblasts were isolated from control and *Col1a1-CreER-CFIm25^{fl/fl}* mice 1 week after the last tamoxifen injection. Cre expression and CFIm25 depletion were confirmed in primary lung fibroblasts isolated from *Col1a1-CreER-CFIm25^{fl/fl}* mice (Figure 5A). Interestingly, this depletion of CFIm25 was associated with significant 3'-UTR shortening of *Col1a1*, *Tgfb1*, *Fzd2*, and *Wnt5a* mRNAs (Figure 5B), as well as an increase in their protein expression (Figure 5A). These data suggest that a similar group of profibrotic genes identified in human lung fibrosis could be regulated by CFIm25-associated APA in mouse fibroblasts and that the 3'-UTR shortening of these genes in CFIm25-depleted mouse lung fibroblasts might lead to enhanced pulmonary fibrosis.

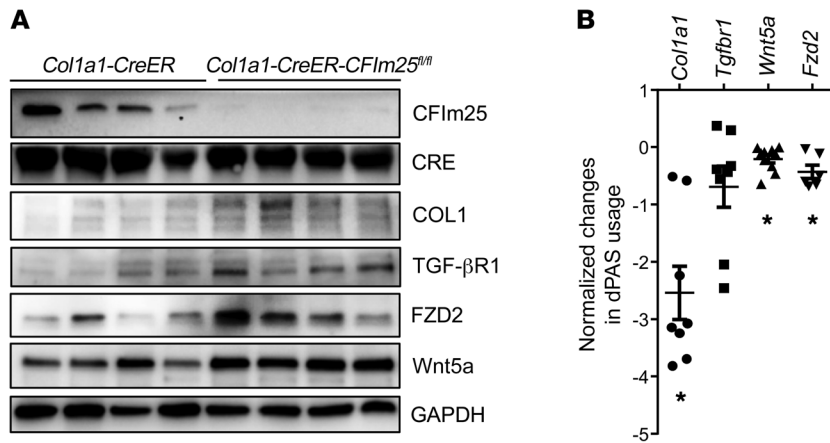


Figure 5. Expression of CFIm25 and its targets in lung fibroblasts isolated from *Col1a1-CreER-CFIm25^{fl/fl}* mice.

Four- to six-week-old *Col1a1-CreER-CFIm25^{fl/fl}* mice and age- and sex-matched littermate controls were administered 75 mg/kg (i.p.) tamoxifen daily for 5 days to induce Cre expression. $n = 4$ biological replications. One week later, fibroblasts were isolated from the lungs of these mice. **(A)** Western blotting was used to confirm the expression of CFIm25, Cre, and CFIm25 targets in fibroblasts, and **(B)** qRT-PCR was performed to determine the dPAS usage of CFIm25 targets (*Col1a1*, *Tgfbf1*, *Fzd2*, and *Wnt5a*). $n = 5$ biological replicates. * $P < 0.05$, by 1-sample t test versus 0.

To directly test this, we exposed these conditional-knockout mice to bleomycin and assessed their pulmonary fibrosis. We observed no mortality in this model of pulmonary fibrosis. *Col1a1-CreER-CFIm25^{fl/fl}* mice exhibited increased COL1 and FN protein expression in association with decreased CFIm25 protein levels in whole-lung lysates (Figure 6A). Consistent with our findings in isolated lung fibroblasts, TGF-βR1, FZD2, and Wnt5A protein expression levels were also increased in the lungs of *Col1a1-CreER-CFIm25^{fl/fl}* mice treated with bleomycin. Less extensive 3'-UTR shortening of *Col1a1* was also observed in bleomycin-treated lungs from *Col1a1-CreER-CFIm25^{fl/fl}* mice compared with that observed in primary fibroblasts (Supplemental Figure 7C). Examination of additional metrics of fibrosis confirmed that there was more lung fibrosis in the lungs of mice in which CFIm25 was knocked out of fibroblasts. For example, transcript levels of *Fnl1* and *Col2a1* were also significantly increased in the lungs of *Col1a1-CreER-CFIm25^{fl/fl}* mice treated with bleomycin (Figure 6, B and C). Moreover, *Col1a1-CreER-CFIm25^{fl/fl}* mice had increased collagen levels in bronchial alveolar lavage (BAL) fluid (Figure 6C). In addition, Masson's trichrome and immunostaining revealed that *Col1a1-CreER-CFIm25^{fl/fl}* mice had increased collagen deposition and an increased number of α-SMA-positive cells (Figure 6D), and blinded Ashcroft scoring confirmed that *Col1a1-CreER-CFIm25^{fl/fl}* mice had exaggerated morphological features of pulmonary fibrosis (Figure 6E). Taken together, these data suggest that deletion of CFIm25 in fibroblasts enhances the expression of profibrotic factors through APA and leads to exaggerated pulmonary fibrosis in mice exposed to bleomycin.

Notably, we detected an increase in total cell numbers as well as in the number of macrophages and lymphocytes in BAL fluid from CFIm25 conditional-knockout mice (Supplemental Figure 7B). Similarly, an earlier examination of the BAL inflammatory profile 7 days after the first bleomycin injection also showed an increase in lymphocytes in CFIm25-depleted mice (Supplemental Figure 8). These findings suggest that CFIm25 depletion may affect inflammation in the early stages of injury response.

Delayed depletion of CFIm25 in late fibrotic stages exaggerates bleomycin-induced pulmonary fibrosis without affecting cellular inflammation. The repeated i.p. bleomycin administration model is initiated with an early inflammatory response and progresses with a late fibrosis stage. The data discussed above show that

CFIm25 depletion before bleomycin injection promotes inflammation. To understand the role of CFIm25 in the late fibrosis stage, Cre activation was delayed to 15 days after the first i.p. bleomycin injection to bypass the CFIm25 depletion in fibroblasts during the early inflammatory stage (Figure 7A). No mortality was observed in the delayed Cre activation of pulmonary fibrosis. We detected a notable decrease in CFIm25 protein and transcript levels in the lungs of knockout mice. No difference in the BAL inflammatory profile was seen between *Col1a1-CreER-CFIm25^{fl/fl}* and control mice (Supplemental Figure 9B). However, pulmonary fibrosis in *Col1a1-CreER-CFIm25^{fl/fl}* mice was worsened, as shown by increased protein and transcript levels of the fibrotic makers COL1 and FN (Figure 7, B and C), elevated soluble collagen levels (Figure 7D), enhanced collagen deposition and myofibroblast numbers (Figure 7F), and a higher Ashcroft score (Figure 7G). In addition, a lung function assay performed using the flexiVent system confirmed that *Col1a1-CreER-CFIm25^{fl/fl}* mice had exaggerated tissue damping, elastance, and resistance as well as decreased compliance and inspiratory capacity, without affecting the Newtonian resistance (Figure 7E). Taken together, our data indicate that depletion of CFIm25 in late fibrotic stages exaggerates bleomycin-induced pulmonary fibrosis without affecting inflammation.

CFIm25 depletion promotes single-dose oropharyngeal bleomycin-induced pulmonary fibrosis. The fibrosis results from the repeated i.p. bleomycin injection model used above are progressive and not resolvable (15–17). In contrast, the single-dose oropharyngeal (o.p.a.) bleomycin instillation model is progressive and resolvable (16, 18). To gain an in-depth understanding of the function of CFIm25 deletion in pulmonary fibrosis, we next examined the role of CFIm25 in the o.p.a. fibrosis model (Figure 8A). We found that removal of CFIm25 before bleomycin injection significantly promoted pulmonary inflammation (Supplemental Figure 10B). Examination of protein and transcript levels of the fibrotic markers COL1a1 and FN1 indicated that lung fibrosis was elevated in mice with CFIm25-depleted fibroblasts (Figure 8, B and C). A Sircol assay showed increased soluble collagen levels in BAL fluid from *Col1a1-CreER-CFIm25^{fl/fl}* mice (Figure 8D) in association with increased tissue elastase and resistance, and decreased compliance and inspiratory capacity (Figure 8E). Moreover, Masson's trichrome and immunostaining indicated increased collagen deposition and an increased number of α-SMA-positive cells in fibro-

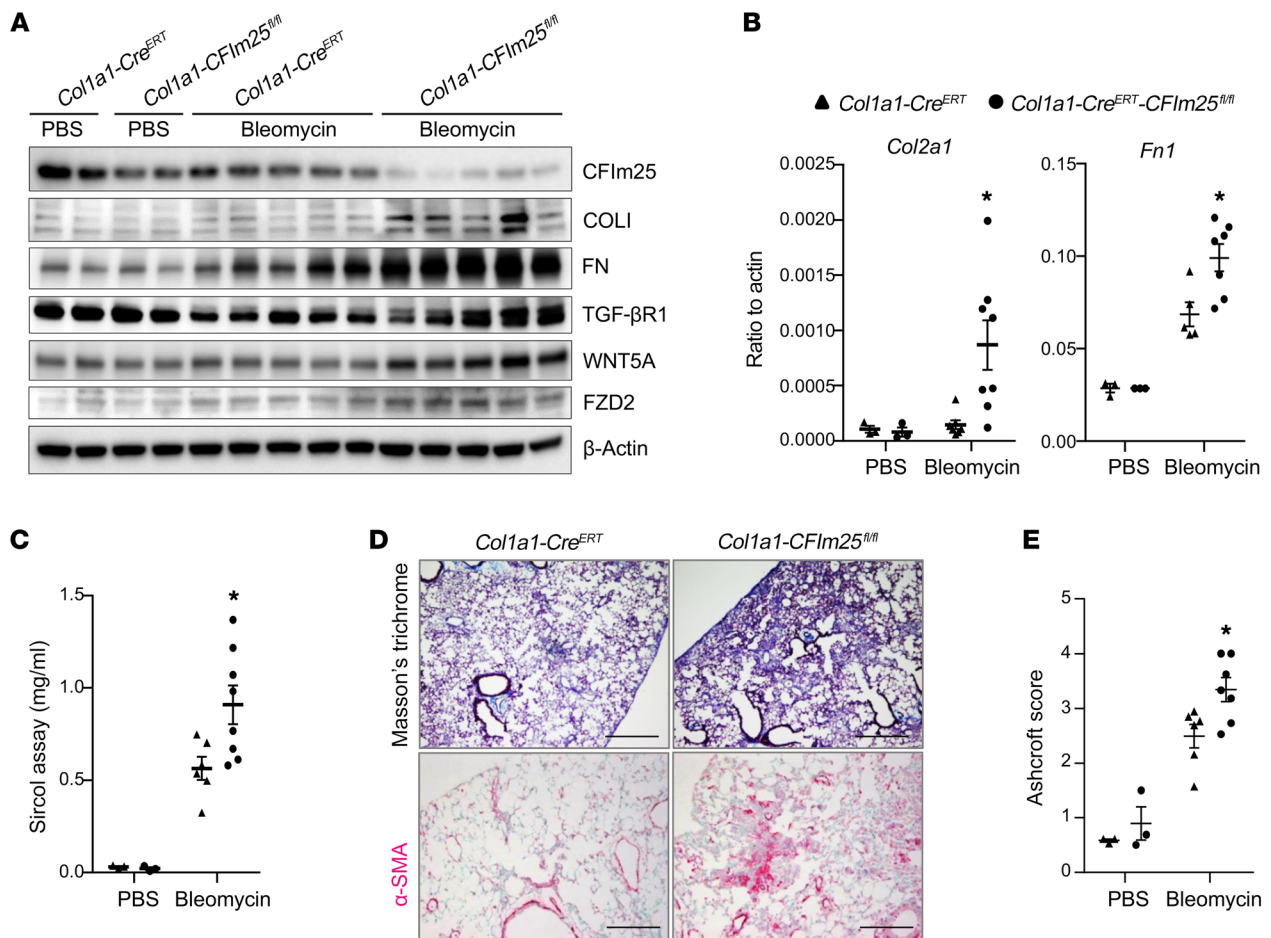


Figure 6. Bleomycin-induced pulmonary fibrosis is exaggerated in *Col1a1-CreER-CFIm25^{fl/fl}* mice. Four- to six-week-old *Col1a1-CreER-CFIm25^{fl/fl}* mice and age- and sex-matched littermate controls were administered 75 mg/kg tamoxifen (i.p.) daily for 5 days to induce Cre expression. After 1 week, the mice were injected with PBS or bleomycin biweekly for 4 weeks. Lungs were collected for analysis 28 days after the first bleomycin injection. (A) Western blot shows CFIm25, COL1, and FN expression in the lungs of control and *Col1a1-CreER-CFIm25^{fl/fl}* mice. Pulmonary fibrosis was analyzed using a Sircol assay (B), qRT-PCR (C), Masson's trichrome and α -SMA staining (D), and an Ashcroft assay (E). * $P < 0.05$, by 1-way ANOVA followed by Bonferroni's multiple comparisons test versus *Col1a1-CreER* mice treated with bleomycin. $n > 4$ biological replicates.

blasts from *Col1a1-CreER-CFIm25^{fl/fl}* mice (Figure 8F). Blinded Ashcroft scoring consistently showed more morphological fibrosis changes in CFIm25 conditional-knockout mice (Figure 8G). Our data suggest that CFIm25 depletion promotes single-dose o.p.a. bleomycin-induced pulmonary fibrosis.

Moreover, to determine the role of CFIm25 during the late fibrotic stage, delayed Cre activation was induced 15 days after the o.p.a. bleomycin instillation (Supplemental Figure 11A). Bypassing CFIm25 deletion during the early inflammatory stage offset the inflammatory difference between the conditional knockout mice and control mice that was observed in the early Cre activation model (Supplemental Figure 11B). Interestingly, pulmonary fibrosis was still augmented, although to a lesser extent compared with the early Cre activation model, in mice with CFIm25-depleted fibroblasts (Supplemental Figure 12). Taken together, our data indicate that depletion of CFIm25 in late fibrotic stages exaggerates o.p.a. bleomycin-induced pulmonary fibrosis without affecting inflammation.

To gain additional evidence for the ability of diminished expression of CFIm25 to affect APA and pulmonary fibrosis in

mice, we also crossed CFIm25-floxed mice with mice expressing Cre driven by the *Foxd1* promoter, which targets progenitor-derived pericytes that have been shown to give rise to a large proportion of active fibroblast in pulmonary fibrosis in mice (19). Interestingly, homozygous deletion of CFIm25 using *Foxd1-Cre* was lethal; however, we were able to analyze heterozygotic (*Foxd1-Cre-CFIm25^{fl/+}*) mice. We detected a reduction of approximately 50% in CFIm25 transcript and protein expression levels in primary fibroblasts isolated from the lungs of *Foxd1-Cre-CFIm25^{fl/+}* mice compared with those from age- and sex-matched littermate controls (Supplemental Figure 13, A and B). In association with the downregulation of CFIm25, a shift from dPAS to pPAS usage was also confirmed for the CFIm25 targets *Fzd2* and *Vma21* (Supplemental Figure 13C). Similarly, when *Foxd1-Cre-CFIm25^{fl/+}* mice were subjected to i.p. bleomycin exposure (Supplemental Figure 14) or one-time o.p.a. bleomycin exposure (Supplemental Figure 15), we observed increased pulmonary fibrosis without any deaths (Supplemental Figure 14 and 15). These results further suggest that downregulation of CFIm25 in fibroblasts or their precursors is associated with increased pulmonary fibrosis.

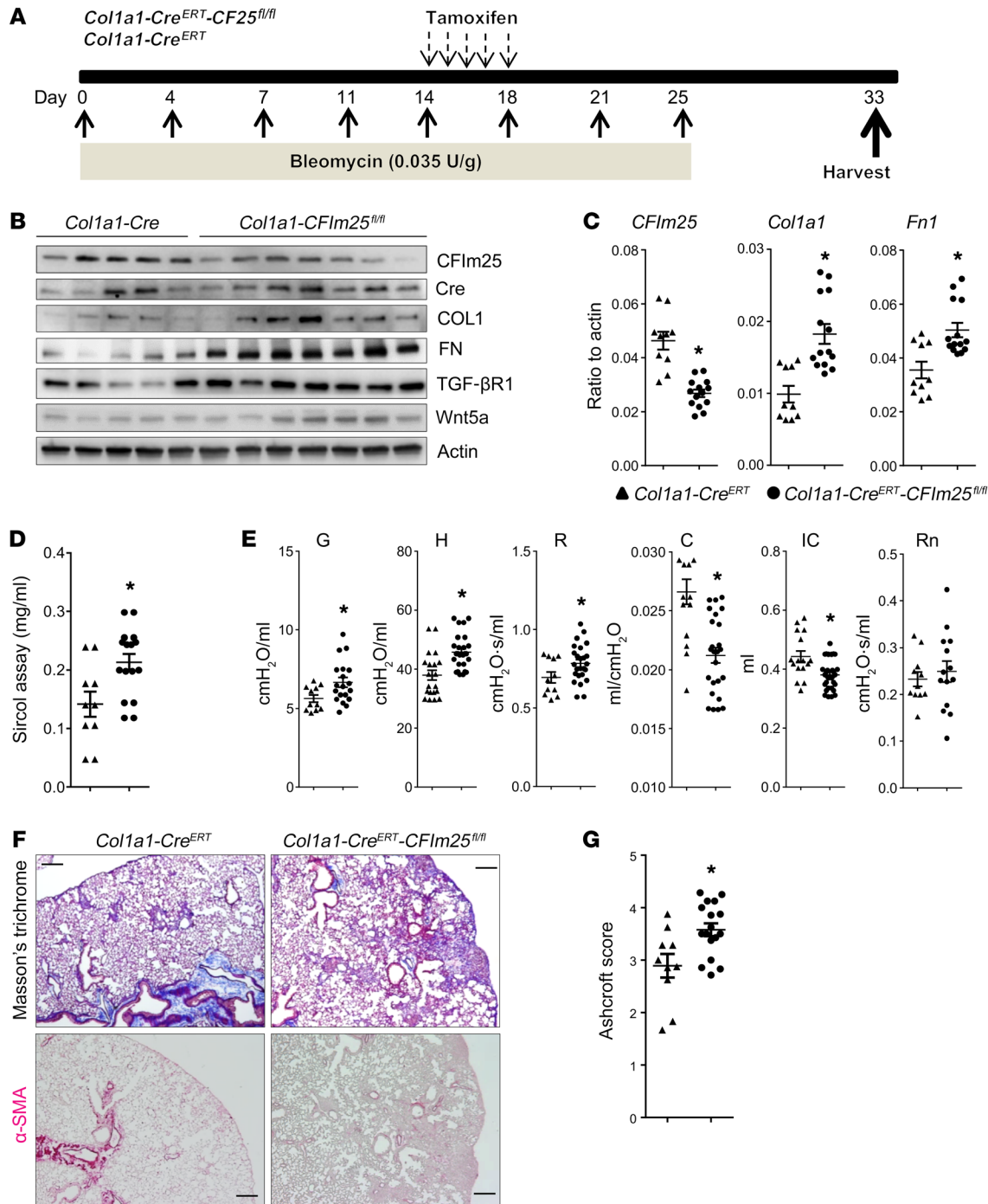


Figure 7. Bleomycin-induced fibrosis is elevated in *Col1a1-CreER-CFIm25^{fl/fl}* mice with delayed Cre activation. (A) Diagram shows the experimental design. Four- to six-week-old *Col1a1-CreER-CFIm25^{fl/fl}* mice and age- and sex-matched littermate controls were i.p. injected with PBS or bleomycin biweekly for 4 weeks. Starting on day 15 after the first bleomycin injection, the mice were i.p. injected with tamoxifen daily for 5 days to induce Cre recombination. Samples were collected for analysis 33 days after the first bleomycin injection. (B) Western blot shows CFIm25, Cre, COL1, FN, TGF-βR1, and Wnt5A expression in the lungs of control and *Col1a1-CreER-CFIm25^{fl/fl}* mice. Levels of pulmonary fibrosis were analyzed using qRT-PCR (C) and a Sircol assay (D). (E) Lung function assay shows the parameters of tissue damping (G), tissue elastance (H), resistance (R), compliance (C), inspiratory capacity (IC), and Newtonian resistance (Rn). (F) Masson's trichrome and α-SMA staining shows collagen deposition and myofibroblast differentiation. Scale bar: 200 μm. (G) The pulmonary fibrosis seen in Masson's trichrome-stained slides was quantified by blinded Ashcroft assay. **P* < 0.05, by unpaired *t* test with equal variance. *n* = 8 biological replicates.

Discussion

IPF is a deadly disease with a high prevalence (14.0–42.7 per 100,000 persons) and low survival rate (20%–40% 5-year survival rate) (1). The proliferation and activation of ECM-producing

myofibroblasts is a central but not yet fully understood process that contributes to the progression of IPF. Thus, the identification of targets that promote abnormal myofibroblast proliferation and differentiation or enhance profibrotic gene expression could prove

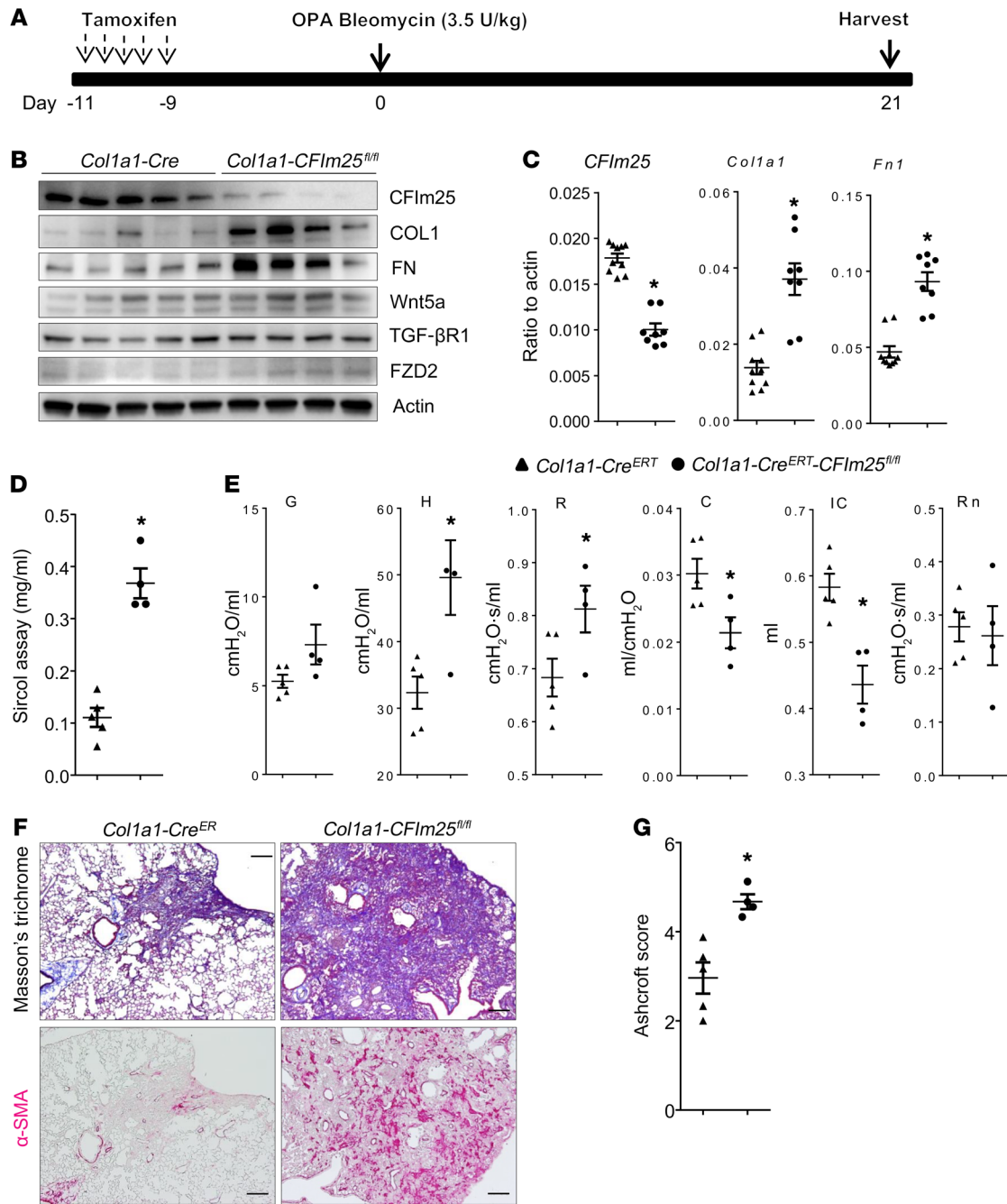


Figure 8. *Col1a1-CreER-CFIm25^{fl/fl}* mice have more severe pulmonary fibrosis upon o.p.a. bleomycin injection. (A) Diagram shows the mouse treatment timeline. Four- to six-week-old *Col1a1-CreER-CFIm25^{fl/fl}* mice and age- and sex-matched littermate controls were administered 75 mg/kg tamoxifen (i.p.) daily for 5 days to induce Cre activation. After 1 week, mice were injected with PBS or bleomycin through o.p.a. instillation. Lungs were collected for analysis 21 days after the first bleomycin injection. (B) Western blot shows CFIm25, COL1, FN, TGF-βR1, Wnt5A, and FZD2 expression in the lungs of control and *Col1a1-CreER-CFIm25^{fl/fl}* mice. qRT-PCR (C) and a Sircol assay (D) were carried out to analyze the levels of pulmonary fibrosis. (E) Tissue damping, tissue elastase, resistance, compliance, inspiratory capacity, and Newtonian resistance were analyzed using the flexiVent system. (F) Masson's trichrome and α -SMA staining indicated collagen deposition and myofibroblast differentiation. Scale bars: 200 μ m. (G) Blinded Ashcroft assays were performed to quantify the pulmonary fibrosis observed on Masson's trichrome-stained slides. * $P < 0.05$, by unpaired t test with equal variance. $n > 4$ biological replicates.

highly beneficial in designing therapies for pulmonary fibrosis. In our study, we explored the expression of a key APA complex in pulmonary fibrosis and showed, for the first time to our knowledge, that there is a significant decrease of CFIm components (CFIm25, CPSF59, and CPSF68) in myofibroblasts from the lungs of patients with IPF and mice with pulmonary fibrosis, suggesting

a possible global 3'-UTR shortening during fibroblast-to-myofibroblast differentiation. In addition, downregulation of CFIm25 was sufficient to shorten the 3'-UTR of profibrotic genes such as *Col1a1* and *Tgfb1*, as well as enhance the translation of key components involved in several profibrotic pathways. Moreover, we also demonstrated exaggerated pulmonary fibrosis upon bleomy-

cin exposure in mice with CFIm25-depleted fibroblasts, suggesting that this mechanism has substantial *in vivo* significance. In summary, our findings uncovered CFIm25 downregulation and enhanced APA as mechanisms contributing to the pathogenesis of pulmonary fibrosis.

With the development of modern sequencing technologies, systemic posttranscriptional processes including alternative RNA splicing (20, 21) have been widely studied as mechanisms for the pathogenesis of IPF. However, whether APA events are present in IPF has not been elucidated. More than 70% of human genes contain more than 1 poly(A) site and are capable of producing mRNA isoforms by APA (6). Global APA events have been involved in many biological processes including differentiation, proliferation, and tumorigenesis. Several fibrosis-related genes have also been reported to have multiple 3'-UTR sizes resulting from APA. TGF- β 1 is known to have 2 different 3'-UTR variants generated from APA, with the short isoform being dominant in various human cell types and organs, as well as having greater reporter protein synthesis when incorporated into the luciferase reporter vector compared with the long isoform (22). PDGF, a potent growth factor that stimulates collagen synthesis and plays an essential role in fibrosis, can also be modulated by APA (23). Moreover, GP130 can generate a soluble isoform through intrinsic APA that inhibits IL-6 *trans*-signaling (24). Despite these findings, genome-wide alternative polyadenylation has not, to our knowledge, been reported in IPF. Our study reveals for the first time to our knowledge that CFIm25, together with the other 2 components of CFIm, CFIm59 and CFIm68, is downregulated in myofibroblasts from the lungs of humans and mice with pulmonary fibrosis. Depletion of CFIm components normally causes 3'-UTR shortening of targeted genes. This was first observed in HeLa cells using Northern blot analysis that targeted 4 genes with more than 1 PAS (9). Later, using RNA-Seq technology, systemic 3'-UTR shortening profiles were observed in cancer cells (8) and stem cells (25) upon CFIm25 knockdown. Similar to these previous findings, our RNA-Seq data identified 808 genes with 3'-UTR shortening and only 29 genes with 3'-UTR lengthening after CFIm25 knockdown, indicating that the role of CFIm25 in lung fibroblasts is to promote the usage of dPASs and favor the production of less stable transcripts. The 808 genes identified included important profibrotic factors involved in TGF- β , Wnt, and HIF-1 α signaling pathways. These findings suggest that 3'-UTR shortening of these factors may be a mechanism that leads to their protein upregulation in fibrotic lungs and subsequently promotes pulmonary fibrosis. The deregulation of CFIm25 in myofibroblasts indicates a presence of global APA events during the pathogenesis of IPF. RNA-Seq to determine the APA profile of IPF lungs and characterize primary fibroblasts isolated from IPF lungs will be important to confirm the presence of APA during the differentiation and fibroproliferation of myofibroblasts.

In addition to directly regulating genes involved in fibrosis, CFIm25 depletion may promote pulmonary fibrosis through several indirect approaches. Notably, if CFIm25 is knocked out in *Colla1*-expressing cells prior to bleomycin treatment, pulmonary inflammation is further increased in mice with CFIm25-depleted fibroblasts (Supplemental Figure 7A, Supplemental Figure 9A, and Supplemental Figure 10A), an event that probably occurs

through activating pathways such as the JAK/STAT3 pathway that are involved in inflammation. STAT3 is normally activated by IL-6 through its receptor IL-6R (15). Wnt5A, through the FZD2 receptor, can also phosphorylate STAT3 and regulate epithelial-to-mesenchymal transition in cancer (26). *IL6* and *JAK2* as well as *WNT5A* and *FZD2* all have 3'-UTR shortening in CFIm25-knockdown cells, suggesting an activation of the STAT3 pathway in CFIm25-depleted cells. Moreover, *Colla1-CreER-CFIm25^{fl/fl}* possibly also induces CFIm25 depletion in other *Colla1*-expressing cells such as osteoblasts and odontoblasts that may affect inflammation (27). The observation that CFIm25 deletion in *Foxd1*-expressing pericytes promotes pulmonary fibrosis without affecting inflammation suggests that depletion of CFIm25 in different cells affects inflammation in diverse ways. Both repeated *i.p.* bleomycin and single *o.p.a.* instillation of bleomycin are inflammation-driven pulmonary fibrosis models, in which bleomycin initially leads to an inflammatory injury response that results in increased ECM deposition and pulmonary fibrosis in later stages (16, 18). Interestingly, delaying Cre activation to 15 days after initial bleomycin injection successfully bypassed the CFIm25 depletion in the early inflammatory stage but still promoted pulmonary fibrosis without affecting the inflammatory profile in both repeated *i.p.* bleomycin administration and *o.p.a.* bleomycin fibrosis models, suggesting that, although inflammation may partially contribute to increased fibrosis in CFIm25 conditional-knockout mice, CFIm25 depletion in fibroblasts is sufficient to promote pulmonary fibrosis without affecting inflammation. In addition to inflammation, CFIm25 deletion may also affect the miRNA pools that are available for gene repression. A large number of miRNAs were found to have lost binding sites as a result of the 3'-UTR shortening event caused by CFIm25 knockdown, and 10 of the top 20 miRNAs are known to be involved in fibrosis or fibroblast proliferation and differentiation. The release of these miRNAs may in turn promote pulmonary fibrosis. Taken together, our data from 2 bleomycin-induced fibrosis models and 2 CFIm25 conditional-knockout mouse models confirmed that CFIm25 deletion, possibly through several approaches, is important in the pathogenesis of pulmonary fibrosis.

It has been demonstrated that APA plays important roles in the regulation of cell proliferation, differentiation, tumorigenesis, animal development, immune response, and neuronal activity (28, 29). A large number of transcripts with short 3'-UTRs are observed during T and B lymphocyte activation (30). Likewise, global 3'-UTR shortening is also present in various transformed cancer cells, as well as in human cancers including colorectal carcinomas and breast and lung cancers (31-33). In contrast to 3'-UTR shortening during cell proliferation and tumorigenesis, widespread 3'-UTR lengthening has been reported during mouse and *Drosophila* embryogenesis (34, 35). From these studies, it seems that 3'-UTR shortening is positively correlated with cell proliferation but negatively correlated with cell differentiation (30). Consistent with this conclusion, CFIm25 siRNA causes global 3'-UTR shortening and greatly increases cancer cell proliferation (8). However, no difference in cell proliferation was observed in CFIm25-depleted stem cells; instead, CFIm25 suppression was found to control cell fate changes (25). Notably, our *in vitro* studies show that proliferation was not enhanced but instead was

suppressed in human lung fibroblasts after CFIm25 depletion (Supplemental Figure 4C), although a similar systematic 3'-UTR shortening was also observed. In addition, the 3'-UTR shortening of proliferation-associated genes (such as cyclin D1), which is normally seen upon CFIm25 deregulation in cancer cells and during cell proliferation, was not observed in human lung fibroblasts after CFIm25 knockdown. The differential effects of CFIm25 depletion on various cells is possibly due to the availability of miRNAs and ARE-binding proteins targeted to these APA genes, or to the presence and cofunction of other APA regulatory factors in human lung fibroblasts. Taken together, these findings suggest that global 3'-UTR shortening could be correlated with either cell proliferation or differentiation and is a cell- and tissue-dependent event.

While our studies focused mainly on CFIm25, other genes were also found to regulate APA in recent studies. Large-scale transcriptome analysis from 2 groups identified 2 genes significantly correlated with 3'-UTR shortening events in malignancies: cleavage stimulation factor subunit 2 (*CSTF64*) (11) and poly(A)-binding protein nuclear 1 (*PABPN1*) (36). Upregulation of *CSTF64* promotes the usage of proximal APA sites in LPS-stimulated macrophages and differentiating B cells (37, 38). In correlation, mammalian polypyrimidine tract-binding protein (PTB), *Drosophila* sex lethal proteins, and RNA-binding protein HuR regulate APA by competing with *CSTF64* and acting as its antagonist (39–41). Loss of cleavage polyadenylation factor subunit FIP1 or PCF11 resulted in global 3'-UTR lengthening in C2C12 mouse cells (42). FIP1 also plays a role in mouse embryonic cell differentiation through APA regulation (43). In as much as our studies identify APA as a new cellular process in pulmonary fibrosis, it will be important to understand whether other APA regulatory factors are involved in the pathogenesis of pulmonary fibrosis. Moreover, in addition to myofibroblasts, it will also be important to examine the expression and function of CFIm components in other cells including epithelial cells, inflammatory cells, and endothelial cells in fibrotic lungs.

Transcripts with shortened 3'-UTRs are generally thought to be more stable and lead to enhanced translation, because miRNAs and RNA-binding proteins (RBPs) that typically repress translation by binding to the 3'-UTR can no longer do so. However a few 3'-UTR RBPs including those of the ELAV protein family could enhance translation (44, 45). Therefore, it is important to emphasize that shorter isoforms are not necessarily more stable as a result of diverse regulation patterns by RBPs and miRNAs (44, 46). This may be the reason why only a small portion of APA genes have increased protein expression after in CFIm25 depletion from stem cells (25). In addition, the 3'-UTR may also act as a sponge for miRNAs; therefore, 3'-UTR shortening of some genes may free up miRNAs that in turn regulate other genes (46). Additional studies are needed to elucidate RNA-protein and RNA-miRNA interactions and assess the impact of APA events in human diseases including pulmonary fibrosis.

Foxd1 perigenitor-derived pericytes are present in the lungs and can expand and differentiate into myofibroblasts upon bleomycin exposure. These cells are the source of more than 50% of α -SMA-expressing cells and are important myofibroblast precursors (19). Our characterization of primary fibroblasts isolated from *Foxd1-Cre-CFIm25^{fl/+}* mice revealed that deletion of CFIm25 in only 1 chromosome of Foxd1 perigenitor-derived pericytes result-

ed in an approximately 50% decrease in transcript and protein levels of CFIm25 and a significant 3'-UTR shortening of CFIm25 targets. Moreover, in agreement with our in vitro findings that CFIm25 depletion promotes fibroblast-to-myofibroblast differentiation, the downregulation of CFIm25 in myofibroblast precursors promoted pulmonary fibrosis by increasing myofibroblast differentiation, collagen and FN synthesis and deposition, as well as scar formation and airway remodeling in a mouse model of pulmonary fibrosis. These findings suggest that CFIm25 downregulation and APA are mechanisms involved in the development of pulmonary fibrosis. Little to nothing is known about the factors that regulate the downregulation of CFIm25, and determining how it is downregulated in fibroblasts during the progression of pulmonary fibrosis could uncover new therapeutic approaches centered on preventing its downregulation and subsequent enhancement of profibrotic pathways.

In conclusion, our study explored the expression of a key APA complex in pulmonary fibrosis and revealed a marked decrease of CFIm components (CFIm25, CFIm59, and CFIm68) in myofibroblasts from the lungs of patients with IPF and mice with pulmonary fibrosis. Moreover, CFIm25 downregulation was sufficient to promote profibrotic gene expression in vitro and exaggerated pulmonary fibrosis in vivo in association with APA. These findings enhance our knowledge of a mechanism of profibrotic gene expression that contributes to the excessive amplification of ECM proteins and other profibrotic factors in deadly fibrotic disorders such as IPF. We believe this research lays the foundation for identifying agents that block this pathway and thereby stop the progression of pulmonary fibrosis and related disorders.

Methods

Cell culture and transfection. Human lung fibroblast lines derived from healthy lungs (CCD8-Lu) or IPF lungs (LL97A) were purchased from the American Type Culture Collection (ATCC). CCD8-Lu cells were cultured in Eagle's Minimum Essential Medium (EMEM) supplement with 10% FBS and antibiotics. LL97A cells were cultured in Ham's F12K medium supplement with 15% FBS and antibiotics. Cells were cultured at 37°C in a humidified 5% CO₂ atmosphere.

For siRNA transfection, cells were cultured in antibiotic-free media, transfected with 50 ng/ml miRNA mimic using Lipofectamine RNAiMAX (Life Technologies, Thermo Fisher Scientific) on day 0 and day 1, and collected for Western blot or qRT-PCR analysis on day 4.

For CFIm25 overexpression, the coding region (CDS) of the human CFIm25 gene was cloned into pCDNA3.1 plasmids (Thermo Fisher Scientific). Six micrograms of empty plasmids or pCDNA3.1-CFIm25 plasmids were electroporated into 5×10^6 healthy or IPF fibroblasts using a capacitor setting of 500 μ F and a voltage of 120 V for 2-mm cuvettes. Transfected fibroblasts were cultured for 2 or 3 days and then collected for protein and RNA analysis.

Human samples. Human explanted lung samples from patients with IPF were deidentified and obtained from the Houston Methodist DeBakey Transplant Center. IPF lung tissue was collected at the time of lung explantation and processed on site within 20 minutes. Healthy human lung tissue samples were obtained from the International Institute for the Advancement of Medicine (IIAM). These tissue samples were collected from lungs that were rejected for transplantation but had no chronic pulmonary disease or contusions. Samples from 14

healthy individuals (age range, 30–63 years) and 27 patients with IPF (age range, 49–72 years) were analyzed in this study, and demographic information, including age, race, health condition, sex, blood type, height, weight, and cause of death, was collected.

Mouse generation and treatment. C57BL/6 mice were purchased from The Jackson Laboratory and maintained in accordance with guidelines of the Animal Welfare Committee at the University of Texas Health Science Center at Houston. Only male mice were used in this study, because IPF is more prevalent in males, and female mice are more resistant to bleomycin-induced fibrosis (49, 50).

Col1a1-CreER-CFIm25^{fl/fl} mice were generated by crossing *CFIm25^{fl/fl}* mice with *Col1a1-Cre/ERT2* mice (stock no. 016241, The Jackson Laboratory). *Foxd1-Cre-CFIm25^{fl/+}* mice were generated by crossing *CFIm25^{fl/+}* (C57/BL6) mice with *Foxd1^{tm1(GFPy/Cre)Amc}* (or *FoxD1^{GC}*) mice (stock no. 012463, The Jackson Laboratory). Sex- and age-matched littermates (either *Foxd1-Cre* or *Col1a1-Cre/ERT2*) were used as controls. Mice were genotyped to confirm the expression of Cre and deletion of the floxed alleles. To induce Cre expression in *Col1a1-CreER-CFIm25^{fl/fl}* mice, the mice were i.p. injected with approximately 75 mg/kg tamoxifen (Sigma Aldrich) once every 24 hours for a total of 5 consecutive days.

To induce pulmonary fibrosis, male mice were i.p. injected with bleomycin (0.035 U/g; Teva Pharmaceutical) twice a week for 4 weeks, for a total of 8 injections. Seven, twenty-eight, or thirty-three days after the initial bleomycin injection, lung tissues and BAL fluid were collected for analysis.

For oropharyngeal aspiration of bleomycin, female mice were lightly anesthetized with isoflurane and administered 2.5 μ /kg bleomycin (o.p.a.) (51). Lungs were then collected for analysis 21 days after bleomycin exposure. Female mice were selected for the o.p.a. bleomycin model, as male mice have been shown to have higher mortality rates and more severe fibrosis than female mice (50).

For delayed Cre activation, mice were injected i.p. with repeated doses of bleomycin (0.035 U/g twice a week for 4 weeks) or o.p.a. with bleomycin (2.5 U/kg). Starting on day 15 after the initial bleomycin injection, the mice were i.p. injected with approximately 75 mg/kg tamoxifen once a day for a total of 5 consecutive days. Then, the samples were collected for analysis on day 33 for the repeated i.p. bleomycin administration model and on day 25 for the o.p.a. bleomycin model.

Lung function assay. Lung function measurements were performed using the flexiVent FX system (SCIREQ Inc.). This system was equipped with the FX1 module and operated by Flexiware version 8.3 software. Baseline ventilation was performed using constant volume ventilation at a tidal volume of 10 ml/kg, frequency of 150 breaths per minute, and a positive end expiratory pressure (PEEP) of 3 cmH₂O. On day 33 (i.p.) or day 25 (o.p.a.), the mice were anesthetized with i.p. injection of 5% Avertin (0.012 ml/g BW). Once a surgical plane of anesthesia was reached, a tracheostomy was performed and the trachea cannulated with an 18-gauge metal cannula with a resistance of approximately 0.2–0.3 cmH₂O·s/ml.

After 1 minute of ventilation, the lungs were inflated to 30 cmH₂O over 6 seconds and returned to normal ventilation for 1 minute. Respiratory mechanics were measured under closed chest conditions by applying a forced oscillatory technique (FOT) to the lungs and measuring flow responses to the applied pressures. Single-compartment mechanics (2.5 Hz; SnapShot-150) oscillation was used to obtain respiratory system resistance (Rrs), dynamic compliance (Crs), and elastance

(Ers), and broad band (1–20.5 Hz; Quick Prime-3) was used to measure Newtonian airway resistance (Rn), tissue damping (G), and tissue elastance (H). This was followed by the generation of a pressure-volume (PV) curve using a ramp-style pressure-driven (PVi-P) maneuver to a maximum of 30 cmH₂O to calculate static compliance (Cst).

Inflammation and cellular differential assay. Mice were anesthetized with Avertin, lungs were lavaged 3 times with 0.4 ml PBS to collect BAL fluid. A hemocytometer was used to determine total cell counts. Aliquots of BAL cells were spun onto microscope slides and stained with Diff-Quik (Dade Behring, B4132-1A) to assess cellular differentials. Once BAL fluid was collected and perfused, the right lobes of the lungs were collected for RNA and protein assays, and the left lobe was pressure inflated, fixed in 10% formalin, and embedded in paraffin. Lung sections (5- μ m-thick) were used for immunostaining and further histological analysis.

Primary mouse fibroblast isolation. To isolate primary fibroblasts from mouse lungs, fresh mouse lungs were perfused, separated under sterile conditions, and excised into approximately 1-mm³ fragments. The fragments were digested in DMEM supplemented with 10 mg/ml dispase (Sigma-Aldrich, D4693) and 20 mg/ml collagenase type I (Gibco, Thermo Fisher Scientific, 9001-12-1) for 3 hours at 37°C, followed by filtration through a 100- μ m, a 40- μ m, and a 15- μ m pore filter to remove undigested tissues. Single cells were then washed to remove the enzyme and cultured for 1 week in DMEM (GeneDepot, CM002-050) supplemented with 10% FCS and penicillin-streptomycin to allow fibroblasts to proliferate and become dominant cell types. Cultured fibroblasts were used for experiments between passages 1 and 3.

Western blot analysis. Western blotting was performed as previously described (52) using primary rabbit anti-CFIm25 antibodies (Proteintech, 10322-1-AP); rabbit anti-Cre recombinase antibodies (Cell Signaling Technology, 15036S); rabbit anti-TGF- β 1 antibodies (Sigma-Aldrich, SAB1300113); mouse anti- β -actin antibodies (Sigma-Aldrich, A2228); rabbit anti-FZD2 antibodies (Thermo Fisher Scientific, 38-4700); rabbit anti-Wnt5A antibodies (Thermo Fisher Scientific, PA5-23178); rabbit anti-CFIm59 antibodies (Proteintech, A301-360A); rabbit anti-CFIm68 antibodies (Proteintech, A301-356A); and mouse anti-GAPDH antibodies (Life Technologies, Thermo Fisher Scientific, AM4300) and then incubated with the corresponding secondary antibodies conjugated to HRP (Cell Signaling Technology, 7076 or 7074). Membranes were developed using Amersham ECL Prime Western Blotting Detection Reagent (GE Healthcare Life Sciences).

RNA-Seq. CCD8-Lu cells were lysed using TRIzol (Life Technologies, Thermo Fisher Scientific), and total RNA was isolated using an RNeasy Mini Kit (QIAGEN). Total RNA-Seq was performed with a HiSeq 2000 (LC Sciences) as previously described (8). This allowed us to capture both gene expression changes and the diversity of transcripts in both coding and noncoding RNA species. Paired-end RNA-Seq was performed to yield a minimal 60 million reads per sample. RNA-Seq gene expression was quantified using RSEM software in combination with a de novo transcriptome assembler (53). The de novo 3'-UTR alterations between control and CFIm25-knockdown cells were identified using the DaPars bioinformatics algorithm as previously described (8, 11). Briefly, we hypothesize that manipulation of CFIm25 can lead to major changes in APA usage, which will result in RNA-Seq density changes near the 3' end of the mRNA. A linear regression model was then used to identify the exact location of the de novo proximal poly(A) site as the optimal fitting point. The

Table 1. Primers used for qRT-PCR

Gene	Forward primer	Reverse primer
Homo_CFM25	TGAAGTTGAAGGACTAAAACGCT	ACCAGTTACCAATGCAATCGTC
Homo_CFM25 long	GGCCAGTTCAGGTGTATTTTG	TTTCCCTCAACAGAACAGCA
Homo_COL1A1	GTGCGATGACGTGATCTGTGA	CGGTGGTTTCTTGGTCGGT
Homo_COL1A1 long	GTGAGGGAGACAGACACCTG	GTGTCTGGGGATTCCAGGAG
Homo_FN1	CCGTGGGCAACTCTGT	TGCGGCAGTTGTCACAG
Homo_FN1 long	TTGCTAGTTTACCGTTCAGAAGT	TTCAATGAAGGAAAGGTGGA
Homo_FZD2	GTGCCATCTATCTCAGCTACA	CTGCATGTCTACCAAGTACGTG
Homo_FZD2 long	CTTTGCTGGTGTGAGAACTCC	ATGGAAGATGGCGAAAAGTACGAG
Homo_TGFBR1	ACGGCGTTACAGTGTCTCTG	GCACATACAAACGGCCTATCTC
Homo_TGFBR1 long	TTTGTGCAGGATTTCTTAGGCTT	GGCTTCTCAGTATCATTCGACTT
Homo_VMA21	GATAAGGCGGCGCTGAACGCACTGC	TGAGCCTTCATTCAGGCCACATACACA
Homo_VMA21 long	CATCTGCACAGCACCTTACAGTTTGC	GAAATGCAGCACATCCAAATCCTCCC
Homo_WNT5A	ATCTTGGTGGTTCGCTAGGTA	CGCCTTCTCCGATGTACTGC
Homo_WNT5A long	GGTAAAGAGAGATGCCGTG	GTGTAAAGTTTGTGTGAACAGGG
Mus_COL1A1	GCTCCTCTTAGGGCCACT	CCACGTCTCACCATTGGGG
Mus_COL1A1 long	GGCAATGTGAAATGTCCCA	ACAGTCCAAGAACCCTCATGT
Mus_COL1A2	AAGGGTGTACTGGACTCCC	TTGTTACCGGATTCTCCTTTGG
Mus_COL2A1	GGGAATGTCTCTGCGATGAC	GAAGGGGATCTCGGGGTTG
Mus_FZD2	CTTCACGGTCACCACCTATTTAG	CGCAATGTAGGCCACTGACA
Mus_FZD2 long	TAGTGTGAGAATCCCAGTTTCCA	CTGGTCTTCAGATCGCTTCTTT
Mus_WNT5A	CAACTGGCAGGACTTTCTCAA	CATCTCCGATGCCGGAAT
Mus_WNT5A long	TGGTCACAGGATTGCTCACAT	GAGAGGGTGAGCCTTTTGTGATT
Mus_TGFBR1	TCTGCATTGCACTTATGCTGA	AAAGGGCGATCTAGTGATGGA
Mus_TGFBR1 long	TACGTCAGAAACACCATGGGA	ACAAAGGCCCAAAAGTACC
Mus_FN1	GCTCAGCAAATCGTGCAGC	CTAGGTAGTCCGTTCCCACT
Mus_ACTA1	GGCTGTATCCCCTCCATCG	CCAGTTGGTAACAATGCCATGT
Homo_ACTA1	CATGTACGTTGCTATCCAGGC	CTCCTTAATGTCACGCACGAT

difference of APA usage between control and CFIm25 knockdown was then quantified as a change in the percentage of the dPAS usage index (Δ PDUI). The significance of the difference of mean PDUIs between the expression levels of short and long 3'-UTRs in 2 samples in each condition was first computed using Fisher's exact test and then further adjusted using the Benjamini-Hochberg (BH) procedure to control for the FDR at a 5% level. Genes with an absolute difference of mean PDUIs of no less than 0.15 and an absolute \log_2 ratio (fold change) of mean PDUIs of no less than 1 were identified as having significantly shifted 3'-UTR events.

The miRNAs that lost their binding site because of the 3'-UTR shortening were identified on the basis of the binding sites predicted from TargetScan as described previously (54). Any miRNA whose binding site was located within the APA-shortening region was considered to be lost. A PDUI difference of 0.15 and an FDR of 0.05 were used as the cutoffs to focus on 808 shortening genes.

qRT-PCR. RNA was treated with DNase and reverse transcribed using iScript Reverse Transcription Supermix (Bio-Rad). qRT-PCR was performed on the LightCycler 96 (Roche) using the primers listed in Table 1, and data were quantified using the comparative Ct method and presented as the mean ratio to β -actin or 18S RNA.

To detect dPAS usage, 2 pairs of primers were designed, with 1 targeting the ORF to represent the total transcript level and the other targeting sequences just before the dPAS to detect long transcripts that used the dPAS. The percentage of dPAS usage was calculated as fol-

lows: $\Delta Ct = Ct_{\text{distal}} - Ct_{\text{total}}$. Data are presented as the fold change normalized to the control, calculated as follows: $\Delta\Delta Ct = \Delta Ct_{\text{average target}} - \Delta Ct_{\text{average of control}}$. The final $\Delta\Delta Ct$ represents \log_2 (percentage of long transcripts in siCFM25/percentage of long transcripts in siControl). A negative $\Delta\Delta Ct$ value indicated that the mRNA had 3'-UTR shortening compared with the control, and this approach was used to quantify APA (8).

Immunohistochemistry and immunofluorescence. Formaldehyde-fixed mouse or human lungs were dehydrated, paraffin embedded, and sectioned (4- μ m thickness). Sections were rehydrated, quenched with 3% hydrogen peroxide, incubated in citric buffer (Vector Laboratories, H-3300) for antigen retrieval, and blocked with the Avidin/Biotin Blocking System (Vector Laboratories, SP-2001) and then 5% normal goat serum.

For double immunohistochemical staining for CFIm25 and α -SMA (Sigma-Aldrich), sections were incubated with antibodies against CFIm25 (1:400, Proteintech, 10322-1-AP) overnight at 4°C and then with ImmPRESS peroxidase-conjugated anti-rabbit antibodies (Vector Laboratories, MP-7401) for 1 hour at room temperature (RT). Slides were then developed with ImmPACT

DAB substrate (Vector Laboratories, SK-4105). After development, the slides were incubated with mouse anti- α -SMA antibodies (1:1000, Sigma-Aldrich, A5228) overnight at 4°C, then incubated with ImmPRESS Alkaline Phosphatase conjugated anti-mouse secondary antibodies (1:1000, Vector Laboratories, MP-5402) for one hour and developed using Vector Red Substrate (Vector Laboratories, SK-5100).

For CFIm25 and α -SMA immunofluorescence dual staining, lung sections were first stained with anti-CFIm25 antibodies and then with ImmPRESS anti-rabbit IgG (Alkine phosphatase, MP-5401) and developed with Vector Red Substrate (Vector Laboratories). The sections were then blocked with normal horse serum and incubated with anti- α -SMA antibodies and Alexa Fluor 488 goat anti-mouse IgG (Thermo Fisher Scientific, A-11001). For CFIm2 and Cre dual staining, lung sections were first incubated with anti-Cre antibodies (Cell Signaling Technology) and then with ImmPRESS anti-rabbit IgG (alkaline phosphatase) and developed with Vector Red Substrate. The sections were then incubated with anti-CFIm25 antibodies and ImmPRESS anti-rabbit IgG (alkaline phosphatase) and developed with Vector Blue Substrate (Vector Laboratories, SK-5300). The slides were finally mounted with ProLong Gold Antifade Mountant with DAPI (Life Technologies, Thermo Fisher Scientific).

Masson's trichrome staining and Ashcroft assay. Masson's trichrome staining was performed using a Trichrome Stain (Masson) Kit (Sigma-Aldrich, HT15-1KT). The Masson's trichrome-stained slides were blindly assigned to 2 different individuals to access the Ashcroft score.

The assay was performed using a modified system of grades (55, 56) obtained by assessing at least 40 randomly chosen areas for each lung.

Statistics. For scientific rigor, all in vitro cell culture experiments were repeated at least 3 times, and each treatment was completed at least in duplicate. For experiments with no more than 2 treatment groups, 2-tailed *t* tests were used to assess whether the means of 2 groups were statistically different from each other. Otherwise, ANOVA was used to determine whether there were significant differences among treatment groups. If so, multiple comparisons were done to determine whether there were significant differences between the 2 treatments. A *P* value of less than 0.05 was considered statistically significant. Results are presented as the mean ± SEM to indicate variability.

Study approval. All mice were maintained in accordance with the guidelines of the Animal Welfare Committee of the University of Texas Health Science Center at Houston. All experimental designs were reviewed and approved by the Animal Welfare Committee (protocol AWC 18-0138). The mice were treated in accordance with NIH and The Center for Laboratory Animal Medicine and Care (CLAMC) at UTHealth. Human lung samples were obtained from the Methodist Hospital Memorial Hermann Transplant Centers. These tissues are archival tissues, and all associated clinical data related to them were deidentified. Methods for the collection and distribution of these tissues were approved by the IRB of Houston Methodist Hospital.

Author contributions

MRB and TW designed the study. TW, JK, NC, CPM, JGM, FL, JD, JH, and SC performed the experiments. TCM isolated the primary healthy and IPF lung fibroblasts. RAT, BAB and SSSJ collected the human samples. TW and CW performed the mouse lung function assays. WL, EJW, YX, LH, LL, and ZX conducted bioinformatics analyses. TW, KAV, SA, KP, HK, and MRB wrote the manuscript.

Acknowledgments

We would like to thank members of the MRB, EJW, HK, and WL laboratories for helpful discussions and Q. Zhu and T. Shan of LC Sciences for their assistance with RNA-Seq. This work was supported by NIH grants to MRB (R01HL70952), WL (R01HG007538 and R01CA193466), and HK (R01HL138510); Cancer Prevention Research Institute of Texas (CPRIT) grants to EJW (RP140800) and LH (RR150085); and an American Heart Association Predoc-toral Fellowship grant to JK (18PRE33960076).

Address correspondence to: Michael R. Blackburn, Department of Biochemistry and Molecular Biology, McGovern Medical School at UTHealth, 6431 Fannin, Houston, Texas 77030, USA. Phone: 713.500.6087; Email: michael.r.blackburn@uth.tmc.edu.

1. Steele MP, Schwartz DA. Molecular mechanisms in progressive idiopathic pulmonary fibrosis. *Annu Rev Med.* 2013;64:265–276.
2. Wolters PJ, Collard HR, Jones KD. Pathogenesis of idiopathic pulmonary fibrosis. *Annu Rev Pathol.* 2014;9:157–179.
3. Chanda D, Otupalova E, Smith SR, Volckaert T, De Langhe SP, Thannickal VJ. Developmental pathways in the pathogenesis of lung fibrosis. *Mol Aspects Med.* 2019;65:56–69.
4. Zank DC, Bueno M, Mora AL, Rojas M. Idiopathic pulmonary fibrosis: aging, mitochondrial dysfunction, and cellular bioenergetics. *Front Med (Lausanne).* 2018;5:10.
5. Todd NW, Luzina IG, Atamas SP. Molecular and cellular mechanisms of pulmonary fibrosis. *Fibrogenesis Tissue Repair.* 2012;5(1):11.
6. Elkon R, Ugalde AP, Agami R. Alternative cleavage and polyadenylation: extent, regulation and function. *Nat Rev Genet.* 2013;14(7):496–506.
7. Di Giammartino DC, Nishida K, Manley JL. Mechanisms and consequences of alternative polyadenylation. *Mol Cell.* 2011;43(6):853–866.
8. Masamha CP, et al. CFIm25 links alternative polyadenylation to glioblastoma tumour suppression. *Nature.* 2014;510(7505):412–416.
9. Kubo T, Wada T, Yamaguchi Y, Shimizu A, Handa H. Knock-down of 25 kDa subunit of cleavage factor Im in HeLa cells alters alternative polyadenylation within 3′-UTRs. *Nucleic Acids Res.* 2006;34(21):6264–6271.
10. Tian B, Hu J, Zhang H, Lutz CS. A large-scale analysis of mRNA polyadenylation of human and mouse genes. *Nucleic Acids Res.* 2005;33(1):201–212.
11. Xia Z, et al. Dynamic analyses of alternative polyadenylation from RNA-seq reveal a 3′-UTR landscape across seven tumour types. *Nat Commun.* 2014;5:5274.
12. Park HJ, et al. 3′ UTR shortening represses tumor-suppressor genes in trans by disrupting ceRNA crosstalk. *Nat Genet.* 2018;50(6):783–789.
13. Wang Y, Yella J, Chen J, McCormack FX, Madala SK, Jegga AG. Unsupervised gene expression analyses identify IPF-severity correlated signatures, associated genes and biomarkers. *BMC Pulm Med.* 2017;17(1):133.
14. Goodwin J, et al. Targeting hypoxia-inducible factor-1 α /pyruvate dehydrogenase kinase 1 axis by dichloroacetate suppresses bleomycin-induced pulmonary fibrosis. *Am J Respir Cell Mol Biol.* 2018;58(2):216–231.
15. Le TT, et al. Blockade of IL-6 Trans signaling attenuates pulmonary fibrosis. *J Immunol.* 2014;193(7):3755–3768.
16. Luo F, et al. Extracellular adenosine levels are associated with the progression and exacerbation of pulmonary fibrosis. *FASEB J.* 2016;30(2):874–883.
17. Baran CP, et al. Important roles for macrophage colony-stimulating factor, CC chemokine ligand 2, and mononuclear phagocytes in the pathogenesis of pulmonary fibrosis. *Am J Respir Crit Care Med.* 2007;176(1):78–89.
18. Moore BB, Hogaboam CM. Murine models of pulmonary fibrosis. *Am J Physiol Lung Cell Mol Physiol.* 2008;294(2):L152–L160.
19. Hung C, et al. Role of lung pericytes and resident fibroblasts in the pathogenesis of pulmonary fibrosis. *Am J Respir Crit Care Med.* 2013;188(7):820–830.
20. Deng N, Sanchez CG, Lasky JA, Zhu D. Detecting splicing variants in idiopathic pulmonary fibrosis from non-differentially expressed genes. *PLoS One.* 2013;8(7):e68352.
21. Nance T, et al. Transcriptome analysis reveals differential splicing events in IPF lung tissue. *PLoS One.* 2014;9(5):e97550.
22. Martin J, et al. Post-transcriptional regulation of Transforming Growth Factor Beta-1 by microRNA-744. *PLoS One.* 2011;6(10):e25044.
23. Dirks RP, Bloemers HP. Signals controlling the expression of PDGF. *Mol Biol Rep.* 1995;22(1):1–24.
24. Sommer J, et al. Alternative intronic polyadenylation generates the interleukin-6 trans-signaling inhibitor sgp130-E10. *J Biol Chem.* 2014;289(32):22140–22150.
25. Brumbaugh J, et al. Nudt21 Controls Cell Fate by Connecting Alternative Polyadenylation to Chromatin Signaling. *Cell.* 2018;172(1-2):106–120.e21.
26. Gujral TS, Chan M, Peshkin L, Sorger PK, Kirschner MW, MacBeath G. A noncanonical Frizzled2 pathway regulates epithelial-mesenchymal transition and metastasis. *Cell.* 2014;159(4):844–856.
27. Kim JE, Nakashima K, de Crombrugge B. Transgenic mice expressing a ligand-inducible cre recombinase in osteoblasts and odontoblasts: a new tool to examine physiology and disease of postnatal bone and tooth. *Am J Pathol.* 2004;165(6):1875–1882.
28. Sun Y, Fu Y, Li Y, Xu A. Genome-wide alternative polyadenylation in animals: insights from high-throughput technologies. *J Mol Cell Biol.* 2012;4(6):352–361.
29. Yeh HS, Yong J. Alternative polyadenylation of mRNAs: 3′-untranslated region matters in gene expression. *Mol Cells.* 2016;39(4):281–285.
30. Sandberg R, Neilson JR, Sarma A, Sharp PA, Burge CB. Proliferating cells express mRNAs with shortened 3′ untranslated regions and fewer microRNA target sites. *Science.* 2008;320(5883):1643–1647.
31. Singh P, et al. Global changes in processing of mRNA 3′ untranslated regions characterize clinically distinct cancer subtypes. *Cancer Res.* 2009;69(24):9422–9430.

32. Lembo A, Di Cunto F, Provero P. Shortening of 3'UTRs correlates with poor prognosis in breast and lung cancer. *PLoS One*. 2012;7(2):e31129.
33. Morris AR, et al. Alternative cleavage and polyadenylation during colorectal cancer development. *Clin Cancer Res*. 2012;18(19):5256–5266.
34. Hilgers V, Perry MW, Hendrix D, Stark A, Levine M, Haley B. Neural-specific elongation of 3' UTRs during *Drosophila* development. *Proc Natl Acad Sci USA*. 2011;108(38):15864–15869.
35. Ji Z, Lee JY, Pan Z, Jiang B, Tian B. Progressive lengthening of 3' untranslated regions of mRNAs by alternative polyadenylation during mouse embryonic development. *Proc Natl Acad Sci USA*. 2009;106(17):7028–7033.
36. Xiang Y, et al. Comprehensive Characterization of Alternative Polyadenylation in Human Cancer. *J Natl Cancer Inst*. 2018;110(4):379–389.
37. Shell SA, Hesse C, Morris SM, Milcarek C. Elevated levels of the 64-kDa cleavage stimulatory factor (CstF-64) in lipopolysaccharide-stimulated macrophages influence gene expression and induce alternative poly(A) site selection. *J Biol Chem*. 2005;280(48):39950–39961.
38. Takagaki Y, Manley JL. Levels of polyadenylation factor CstF-64 control IgM heavy chain mRNA accumulation and other events associated with B cell differentiation. *Mol Cell*. 1998;2(6):761–771.
39. Castelo-Branco P, Furger A, Wollerton M, Smith C, Moreira A, Proudfoot N. Polypyrimidine tract binding protein modulates efficiency of polyadenylation. *Mol Cell Biol*. 2004;24(10):4174–4183.
40. Gawande B, Robida MD, Rahn A, Singh R. *Drosophila* sex-lethal protein mediates polyadenylation switching in the female germline. *EMBO J*. 2006;25(6):1263–1272.
41. Dai W, Zhang G, Makeyev EV. RNA-binding protein HuR autoregulates its expression by promoting alternative polyadenylation site usage. *Nucleic Acids Res*. 2012;40(2):787–800.
42. Li W, et al. Systematic profiling of poly(A)+ transcripts modulated by core 3' end processing and splicing factors reveals regulatory rules of alternative cleavage and polyadenylation. *PLoS Genet*. 2015;11(4):e1005166.
43. Lackford B, et al. Fip1 regulates mRNA alternative polyadenylation to promote stem cell self-renewal. *EMBO J*. 2014;33(8):878–889.
44. Szostak E, Gebauer F. Translational control by 3'-UTR-binding proteins. *Brief Funct Genomics*. 2013;12(1):58–65.
45. Matoulkova E, Michalova E, Vojtesek B, Hrstka R. The role of the 3' untranslated region in post-transcriptional regulation of protein expression in mammalian cells. *RNA Biol*. 2012;9(5):563–576.
46. Gupta I, et al. Alternative polyadenylation diversifies post-transcriptional regulation by selective RNA-protein interactions. *Mol Syst Biol*. 2014;10:719.
47. Raghu G, Weycker D, Edelsberg J, Bradford WZ, Oster G. Incidence and prevalence of idiopathic pulmonary fibrosis. *Am J Respir Crit Care Med*. 2006;174(7):810–816.
48. King TE, Pardo A, Selman M. Idiopathic pulmonary fibrosis. *Lancet*. 2011;378(9807):1949–1961.
49. Lederer DJ, Martinez FJ. Idiopathic Pulmonary Fibrosis. *N Engl J Med*. 2018;379(8):797–798.
50. Redente EF, et al. Age and sex dimorphisms contribute to the severity of bleomycin-induced lung injury and fibrosis. *Am J Physiol Lung Cell Mol Physiol*. 2011;301(4):L510–L518.
51. De Vooght V, Vanoirbeek JA, Haenen S, Verbeken E, Nemery B, Hoet PH. Oropharyngeal aspiration: an alternative route for challenging in a mouse model of chemical-induced asthma. *Toxicology*. 2009;259(1-2):84–89.
52. Weng T, et al. Hypoxia-induced deoxycytidine kinase expression contributes to apoptosis in chronic lung disease. *FASEB J*. 2013;27(5):2013–2026.
53. Li B, Dewey CN. RSEM: accurate transcript quantification from RNA-Seq data with or without a reference genome. *BMC Bioinformatics*. 2011;12:323.
54. Agarwal V, Bell GW, Nam JW, Bartel DP. Predicting effective microRNA target sites in mammalian mRNAs. *Elife*. 2015;4:e05005.
55. Ashcroft T, Simpson JM, Timbrell V. Simple method of estimating severity of pulmonary fibrosis on a numerical scale. *J Clin Pathol*. 1988;41(4):467–470.
56. Hübner RH, et al. Standardized quantification of pulmonary fibrosis in histological samples. *BioTechniques*. 2008;44(4):507–511, 514.